Resonance properties of different neuronal populations in the immature mouse neocortex

Dissertation

Zur Erlangung des Grades
Doktor der Naturwissenschaften

Am Fachbereich Biologie
Der Johannes Gutenberg-Universität Mainz

vorgelegt von

Haiyan Sun

geb. am 10.08.1981 in Jiangsu China

Mainz, 2013

Tag der mündlichen Prüfung: 29 . May . 2013

Table of Contents

Table of Contents 1

List of figures 3

Abbreviations 5

1. Introduction 7

1.1 Different frequency band oscillations in brain regions 7
1.2 Oscillatory activity patterns contribute to diverse brain functions 9
1.3 Early neuronal activity patterns (delta brushes) in the developing cerebral cortex of humans and rodents 12
1.4 Intrinsic cellular resonance properties contribute to the synchrony oscillations. 15
1.5 Different cellular mechanisms contribute to the resonance 17
1.6 Neuronal resonance in brain regions 20
1.7 Different locations, morphologies and functions of neuronal populations in cerebral cortex 21
1.8 Aims of the thesis 26

2 Materials and Methods 28

2.1 Slice preparation 28
2.2 Electrophysiological recordings 28
2.3 Identification of cells 30
2.4 Characterization of electrical resonance 32
2.5 Solution and Drugs 33
2.6 Statistics 33

3. Results 34

3.1 Properties and mechanisms of subthreshold resonance in Cajal-Retzius cells 34
3.2 Properties and mechanisms of subthreshold resonance in supragranular pyramidal neurons 39
3.3 Properties and mechanisms of subthreshold resonance in layer V pyramidal neurons 44
3.4 Properties of subthreshold resonance in subplate neurons 50
3.5 Electrical properties of immature cortical GABAergic interneurons 52
3.6 Properties of subthreshold resonance in GABAergic interneurons 53
3.7 Role of t-type Ca^{2+} currents for resonance of GABAergic interneurons 55
3.8 Role of hyperpolarization-activated cation currents for subthreshold resonance 56
3.9 Role of persistent sodium currents for subthreshold resonance 57

4. Discussion 60

4.1 Age-dependent electrophysiological properties of a variety of neuronal populations in the immature mouse neocortex *60*
4.2 Resonance properties of different neuronal populations *62*
4.3 Leak conductance may influence the resonance properties of neurons. *63*
4.4 Mechanisms of subthreshold resonance *64*
4.5 Subthreshold resonance increases the cutoff frequency of the immature neurons. *66*
4.6 Resonance properties of single neurons may contribute to the low frequency of oscillatory patterns in the early neuronal networks *67*
4.7 Resonance behaviors of single neurons may contribute to synaptic filtering *68*

5. Summary 69

Reference List 71

Acknowledgments 90

List of figures

Fig. 1 EEG rhythms in humans. 9
Fig. 2 Schematic diagram illustrating oscillatory activity patterns are critical for a variety of brain functions. 12
Fig. 3 Early patterns of electrical activity in the developing cerebral cortex of humans and rodents. 14
Fig. 4 Similar frequencies observed both in spontaneous oscillations and resonance behaviour. 16
Fig. 5 Different locations and morphologies of cortical neurons. 25
Fig. 6 Identification of typical neuronal cell populations in the immature cerebral cortex and analyses of intrinsic resonance properties. 31
Fig. 7 Properties of subthreshold resonance in Cajal-Retzius cells. 36
Fig. 8 Role of h current for subthreshold resonance of Cajal-Retzius cells. 38
Fig. 9 Properties of subthreshold resonance in immature pyramidal neurons of supragranular neocortical layers. 40
Fig. 10 Voltage independence of resonance behaviour in immature pyramidal neurons of supragranular neocortical layers. 41
Fig. 11 H current is not involved in subthreshold resonance of immature pyramidal neurons of supragranular neocortical layers. 42
Fig. 12 Role of t-type Ca^{2+} currents for subthreshold resonance in immature pyramidal neurons of supragranular neocortical layers. 44
Fig. 13 Properties of subthreshold resonance in immature pyramidal neurons of layer V. 46
Fig. 14 Voltage dependence of resonance behaviour in immature pyramidal neurons of layer V. 47
Fig. 15 Role of h current for subthreshold resonance in immature pyramidal neurons of layer V. 49
Fig. 16 Properties of subthreshold resonance in subplate neurons. 51
Fig. 17 Identification of GABAergic interneurons in the immature cerebral cortex. 53

Fig. 18 Properties of subthreshold resonance in GABAergic interneurons. 54

Fig. 19 Role of t-type Ca^{2+} currents for subthreshold resonance of GABAergic interneurons. 56

Fig. 20 The hyperpolarization-activated current (I_h) is not involved in subthreshold resonance of GABAergic interneurons. 57

Fig. 21 Role of persistent Na^{+} currents for the subthreshold resonance of GABAergic interneurons. 59

Abbreviations

α	alpha frequency range (8-13 Hz)
β	beta frequency range (13-30 Hz)
γ	gamma frequency range (30-100 Hz)
δ	delta frequency range (0.5-4 Hz)
θ	theta frequency range (4-7 Hz)
ACSF	artificial cerebrospinal fluid
CA1	Cornu Ammonis area 1
C_{input}	input capacitance
CP	cortical plate
CR	Cajal-Retzius
DIC	differential interference contrast
EEG	electroencephalography
Fig.	Figure
f_{res}	resonance frequency
GABA	γ-aminobutyric acid
HCN	hyperpolarization-activated cyclic nucleotide-gated
Hz	Hertz
I_h	hyperpolarization-activated cation currents
I_{NaP}	persistent Na^+ currents
LTP	long-term potentiation
LTD	long-term depression
MZ	marginal zone
P	postnatal day
PS	pallial septum
Q	maximal impedance amplitude
REM	rapid eye movement
R_{in}	input resistance
RMP	resting membrane potential

SEM	standard error of the mean
SP	subplate
SVZ	subventricular zone
SWS	slow-wave sleep
TTX	tetrodotoxin
VP	ventral pallium
VZ	ventricular zone
ZAP	impedance-amplitude profile
ZD7288	4-Ethylphenylamino-1,2-dimethyl-6-methylaminopyrimidin chloride
Z_f	impedance at the frequency f
Z_0	steady state impedance

1. Introduction

1.1 Different frequency band oscillations in brain regions

Neural oscillation is rhythmic or repetitive neural activity in the central nervous system. Neural tissue can generate oscillatory activity in many ways, driven either by mechanisms localized with individual neurons or by interactions between neurons. In individual neurons, oscillations can appear either as oscillations in membrane potential or as rhythmic patterns of action potentials, which then produce oscillatory activation of post-synaptic neurons. However, in groups of neurons oscillatory activity generally arises from feedback connections between the neurons that result in the synchronization of their firing patterns. When neurons synchronize and resonate with precision in the millisecond range, the field potentials show certain frequency bands of oscillations (Buzsaki and Draguhn, 2004), which can be divided into five major frequency bands: delta (δ, 0.5-4 Hz), theta (θ, 4-8 Hz), alpha (α, 8-13Hz), beta (β, 13-30 Hz) and gamma (γ, 30-100 Hz) (**Fig. 1**). These different frequency oscillatory patterns are typical for a variety of brain functions and involved in brain state determination, sensory perception, memory retrieval or consciousness (Engel et al., 2001;Buzsaki and Draguhn, 2004;Hasselmo, 2005).

Delta waves are high amplitude brain wave with a frequency of oscillation between 0.5-4 Hz, and are in mature mammals usually associated with slow-wave sleep (SWS), also known as non-REM (rapid eye movement) sleep (Sejnowski and Destexhe, 2000). However, they are a dominant brain-wave pattern in infants and immature animals (Hanganu-Opatz, 2010;Kilb et al., 2011). Delta waves can be generated either in the thalamus or in the cortex. In the thalamus, they arise in coordination with the reticular formation (Maquet et al., 1997). In the cortex, the suprachiasmatic nuclei have been shown to regulate delta waves. For example, the lesion to this area has been shown to cause disruptions in delta wave activity. T- type calcium channels have been reported to mediate delta waves (Lee et al., 2004).

The theta (θ) frequency band (4-8 Hz) oscillation is a prominent feature of the

network activity in the hippocampus (Vanderwolf, 1988;Vinogradova, 1995;Buzsaki, 2002). In rodents, the hippocampal θ rhythm is prominent during exploration, locomotion and rapid eye movement (REM) sleep (Bland, 1986;Vanderwolf, 1988;Vinogradova, 1995;Buzsaki, 2002). θ rhythm plays an important role in sensory-motor behaviour, learning and memory processes and synaptic plasticity (Winson, 1978;Huerta and Lisman, 1993;Wilson and Mcnaughton, 1994;Buzsaki, 2002). However, in humans, by EEG or MEG recording in cerebral cortex and hippocampus, θ band oscillations are not involved in exploration or learning, but particularly evident during drowsiness, poor decision making and Fuzzy thinking (Sarnthein et al., 1998;Raghavachari et al., 2001;Kahana et al., 2001).

Alpha waves are neural oscillations in the frequency range of 8-13 Hz and were first discovered by Hans Berger (Hans Berger, 1929). These frequency band oscillations have been suggested to indicate a wakeful period during sleep. Alpha waves are associated with relaxed wakefulness and are enhanced in the visual cortex when the eyes are closed (Buzsaki, 2006). Moreover, these waves have also been observed over the motor cortex (central scalp), which are reduced with movement, or the intention to move (Kolev et al., 1994).

Beta wave is the frequency range of human brain activity between 13 and 30 Hz. These frequency band oscillations have been found in the motor cortex, where they are suggested to contribute to the motor control and movement changes (Lalo et al., 2007;Baker, 2007). In addition, beta states are associated with normal waking consciousness. Furthermore, low amplitude beta waves with multiple and varing frequencies are often associated with active, busy, or anxious thinking and active concentration (Baumeister et al., 2008).

A gamma wave is a pattern of neural oscillation in humans with a frequency between 30 to 100 Hz (Hughes, 2008), although 40 Hz is typical (Gold, 1999). In adult human motor cortex, gamma band activity prevails during a sensorimotor task by magnetoencephalographic recordings (Tecchio et al., 2008). Gamma rhythm has been observed during attention, learning, and perception (Engel et al., 2001). In the immature rodents neocortex oscillatory activity patterns gamma range (30-100 Hz)

are observed already in the first postnatal week (Engel et al., 2001;Dupont et al., 2006;Yang et al., 2009;Brockmann et al., 2011;Minlebaev et al., 2011;Yang et al., 2012). These oscillations are not only involved in coordinated information processing, but may also contribute to the development of adequate neuronal projections and local circuits (Khazipov and Luhmann, 2006;Hanganu-Opatz, 2010).

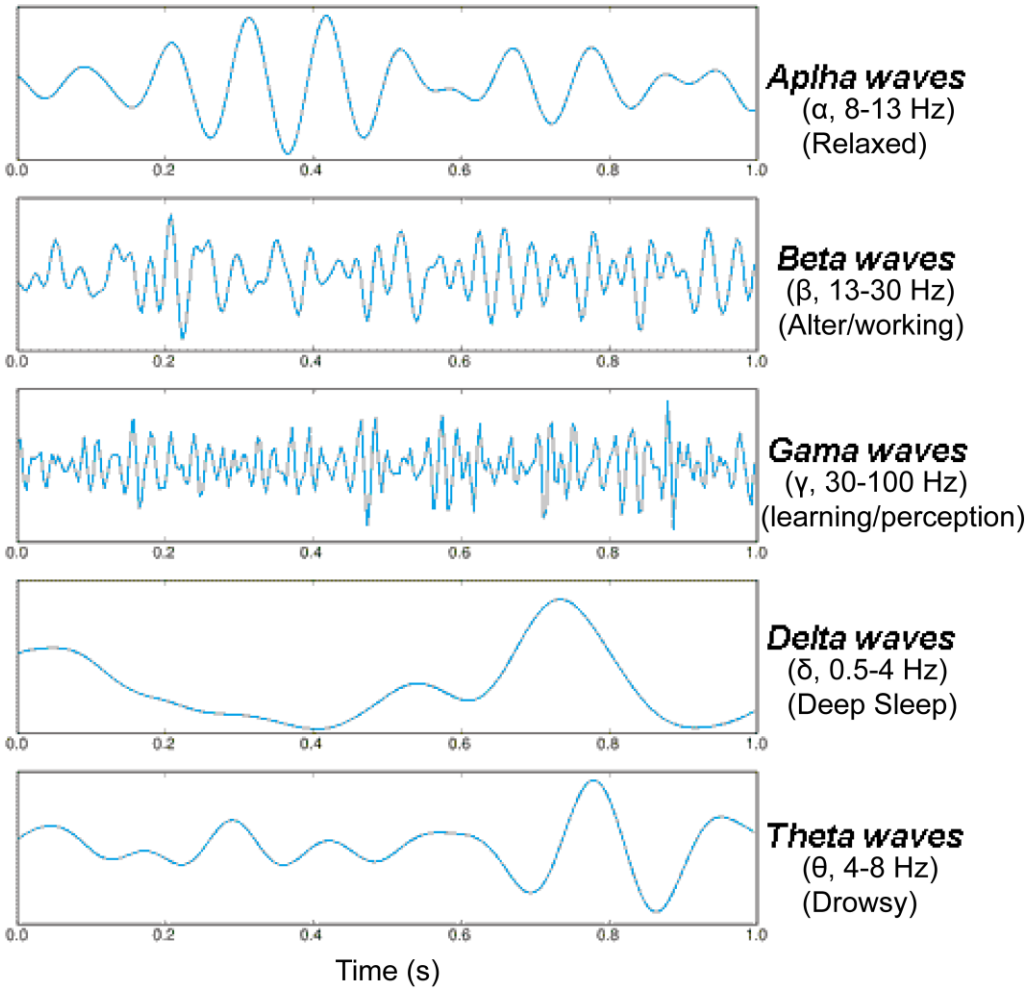

Fig. 1 EEG rhythms in humans.

Depending on the brain's state the EEG differs in amplitude and frequency. Picture modified from http://www.docgautham.com/causes/brain_waves.

1.2 Oscillatory activity patterns contribute to diverse brain functions

Oscillatory activity patterns are crucial for a variety of brain functions, such as brain state determination, sensory perception, motor output, memory encoding, retrieval, and the development of neuronal circuits and functional sensory

topography map (Engel et al., 2001;Buzsaki and Draguhn, 2004;Hasselmo, 2005;Khazipov and Luhmann, 2006) (**Fig. 2**). The whole brain oscillations determine the switch between sleep and awake states and make them re-occur about every 24 hours. The changes of environment initiate the whole process. Firstly, different visual stimulus by light intensity drives the phase of ongoing brain oscillations. Meanwhile, the different aspects of the stimulus are encoded in various frequencies oscillations. Then, all these oscillations affect brain processes and the intrinsic circadian clock. Finally, the circadian clock triggers this periodicity. During awake state oscillating neuronal populations modulate communication by integrating the sensorimotor information and transferring the information flow. In contrast, during the sleep period, thalamocortical spindle oscillations effectively reduce environmental influences on neocortical activity, thereby actively shifting sleep into deeper stages. In summary, oscillatory activity patterns triggered by sensory information can change the intrinsic circadian rhythms (for review, see Thut et al., 2012).

Oscillatory activity patterns contribute to the sensory perception in brain. Sensory periphery input is detected and selected basing on single neuron intrinsic resonance frequency characteristics. Input frequency preference can be dynamically tuned by biasing the membrane conductance and potential. Moreover, cortical interneuron classes have a wide range of preferred frequencies, which enable themselves to set diverse network dynamics. On the other hand, these oscillations can be amplified from weak signals to the strong information flow with help of the sub-cortical regions. For example, the thalamus can amplify the thalamocortical oscillations by the cortical feedback to it. Furthermore, the sensory information in the brain was continued to be processed, transferred and stored by neuronal assemblies which can synchronized by oscillation. The oscillations enable the distant cortical regions with different neuronal assemblies to link together temporally. Finally, the sensory information can be processed to be consolidation and combination of memory information by the activating the diverse assemblies (Buzsaki and Draguhn, 2004).

Memory encoding and retrieval depends on theta oscillations in hippocampus.

Theta oscillations are associated with laminar segregation of rhythmic sources and sinks in region CA1 and dentate gyrus. Current source density analysis from the local field potential supports the model of phases of encoding and retrieval. The phasic changes in current sinks result from the synaptic transmissions. In vitro studies revealed that stimulation on the peak of theta wave causes LTP, while stimulation on the trough causes long-term depression (LTD). LTP is strong during encoding period, and then LTP becomes weak during retrieval period (Hasselmo, 2005).

Moreover, these oscillations have been suggested to play critical roles in refinement and maturation of early neuronal cortical circuits and functional topography map in the different sensory systems during the early development (Khazipov and Luhmann, 2006). In the somatosensory system, spindle bursts (intermittent network bursts associated with spindle-shape field oscillations) in S1 have been reported to shape the formation of cortical connections required for sensorimotor coordination. Moreover, these oscillations in S1 driven by the spontaneous paws twitches contribute to the formation of the somatotopic sensory cortical map (Khazipov et al., 2004). In the whisker system, gamma and spindle bursts modulate both thalamic-cortico and cortico-thalamic network loops (Minlebaev et al., 2011;Yang et al., 2012). In addition, the precise topographic and functional columnar organization in barrel cortex also needs the localized gamma and spindle bursts in neonatal vibrissal S1 (Yang et al., 2012) induced by the spontaneous whisker movements (Tiriac et al., 2012). In the visual system, the patterned spontaneous retinal waves not only contribute to the retinotopic map refinement in the superior colliculus (McLaughlin et al., 2003;Chandrasekaran et al., 2005), but also trigger spindle bursts (Hanganu et al., 2006) required for the development of precise maps in V1 (Cang et al., 2005). In the auditory system, spontaneous activity in auditory nerve fibers before the onset of hearing is essential for the refinement and maintenance of tonotopic maps in the developing auditory system (Gabriele et al., 2000;Rubel and Fritzsch, 2002;Kandler, 2004;Leake et al., 2006;Leao et al., 2006;Tritsch et al., 2007).

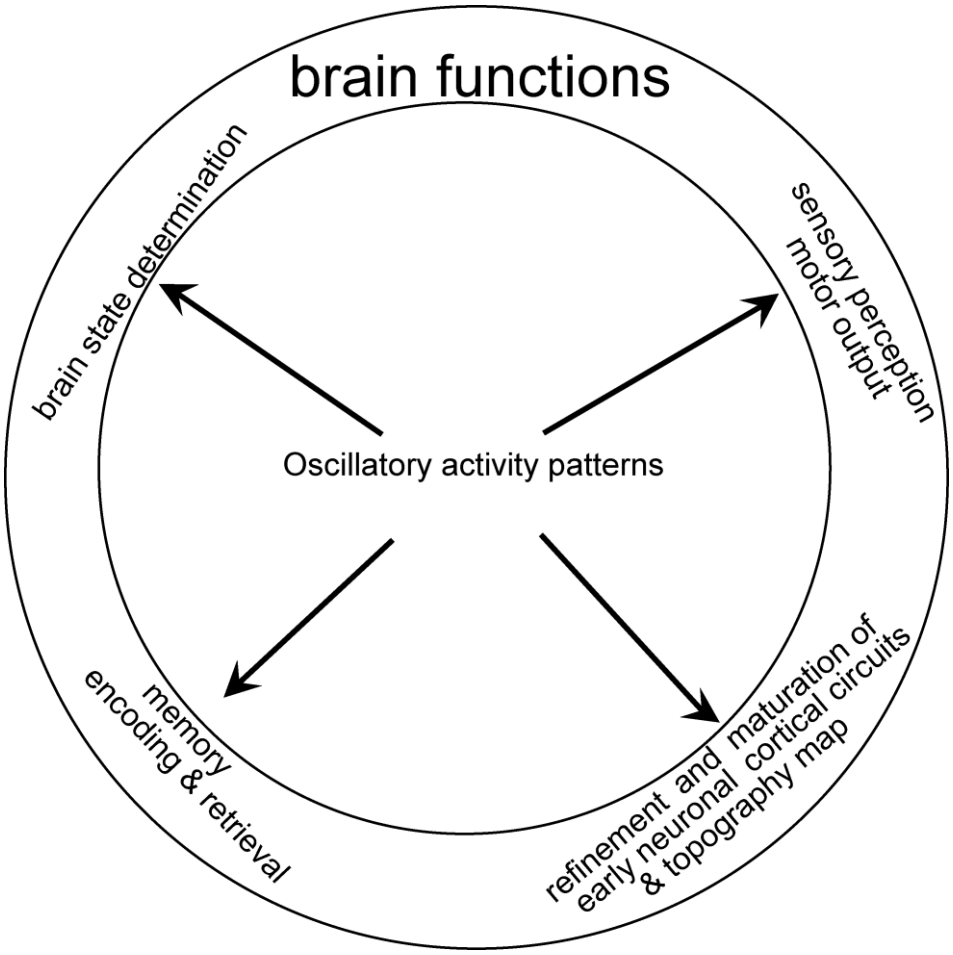

Fig. 2 Schematic diagram illustrating oscillatory activity patterns are critical for a variety of brain functions.

1.3 Early neuronal activity patterns (delta brushes) in the developing cerebral cortex of humans and rodents

By electroencephalogram (EEG) recording, highly intermittent temporal bursts were found in human premature neonates (Khazipov and Luhmann, 2006). These early neocortical patterns called delta brushes are prominent at mid-gestation (Anderson et al., 1985;Lamblin et al., 1999;Khazipov and Luhmann, 2006). About 0.3-2.0 Hz delta band dominates in the patterns activity. Later with increase of age, the suppression of these patterns becomes more prominent. By the seventh month of gestation, slow oscillations are intermixed with rapid rhythms. During this period, each event consists of slow waves at about 0.3-1.5 Hz delta band and rapid

component at 8-25 Hz alpha band (**Fig. 3A-B**), which corresponding to spindle bursts. After birth, still some discontinuous patterns can be observed but with low occurrence. The patterns of activity completely disappear in the mature cortex. Furthermore, in preterm infants, delta brushes have been suggested to serve as a criterion of normal development. Their absence is considered an indicative of brain pathology and poor prognosis (Holmes and Lombroso, 1993).

Similarly, in the neonatal rats, delta brushes can be also observed by extracellular multielectrode recording (**Fig. 3C**)(Colonnese et al., 2010;Colonnese and Khazipov, 2010). In the neonatal primary visual cortex, the delta brushes consisting of slow waves and high-frequecy oscillations occurred spontaneously at P7 and younger rats before eyes opening (**Fig. 3D**). Then two days later, sensory evoked responses could be induced in visual cortex by light flashes (**Fig. 3E-F**). This responses consist of the slow activity transients which has about 1-3 s duration and large (>1 mV) negative local-field potentials. In the large negative waves, there are summations of multiple bursts of rapid oscillations in the high beta and gamma bands. Surprisingly, these patterns of activity can't be observed anymore after eye opening (**Fig. 3G-H**). Colonnese and colleague proposed that the synchronous delta brushes participate in the formation of visual circuitry (Colonnese and Khazipov, 2010).They also suggested that the early development of visual processing is governed by a conserved, intrinsic program that switches thalamocortical response properties in anticipation of patterned vision (Colonnese et al., 2010).

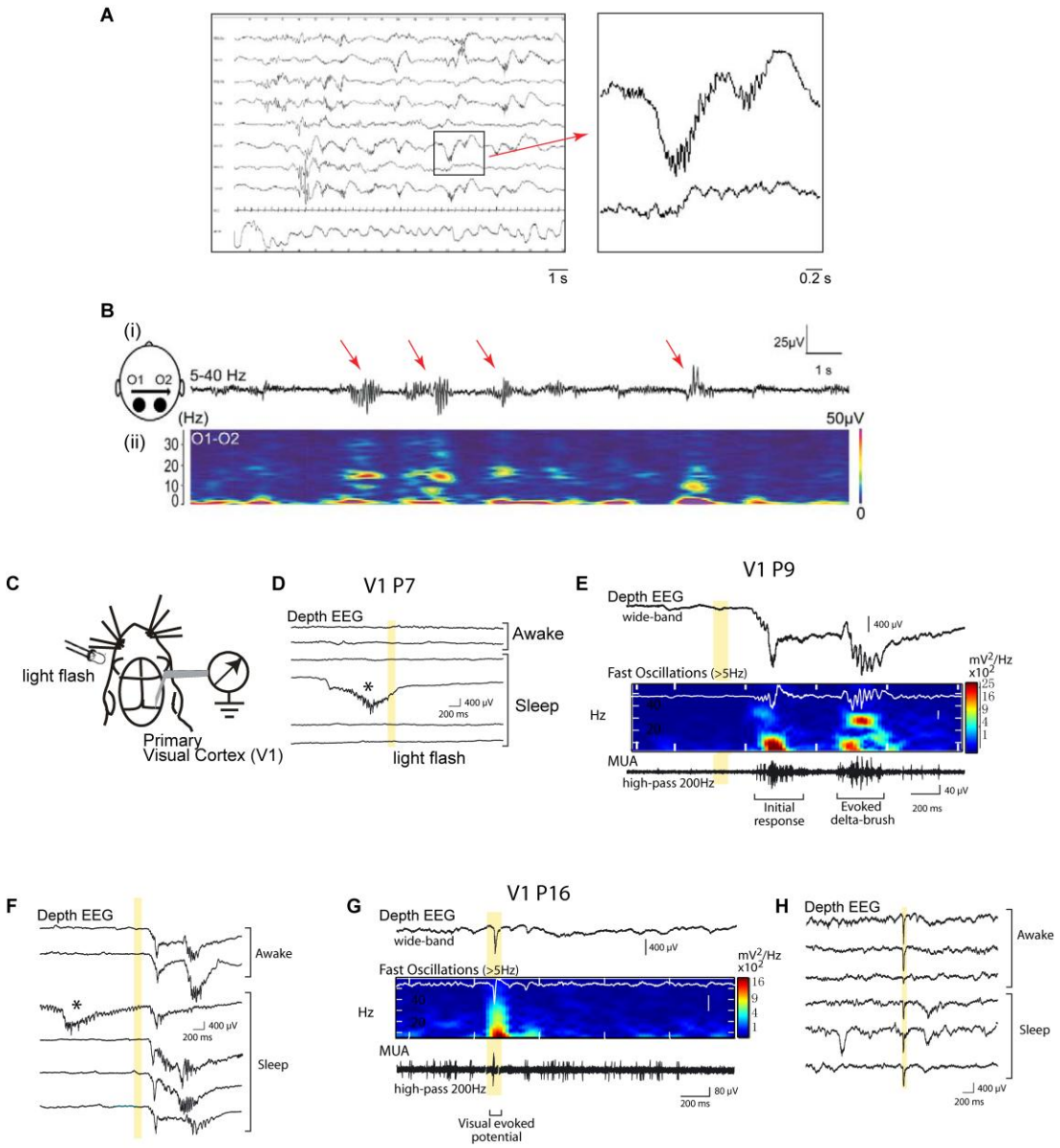

Fig. 3 Early patterns of electrical activity in the developing cerebral cortex of humans and rodents.

A. EEG recording in a premature human neonate aged 33 weeks. Note that typical patterns of activity consist of delta waves (1–3 Hz) that grouped high-frequency oscillations. An example delta brush is shown at an expanded timescale on the right. **B.** Bipolar occipital (O1–O2) recordings **(i)** from the visual cortex of a premature neonate (filtered at bandpass 5–40 Hz) and corresponding spectrogram **(ii)**. Note the slow and rapid components of delta brushes (marked by red arrows). **C-H.** Three periods in the early development of visual stimulation in the rat. **C.** Schematic diagram of the experimental setup illustrating visual stimulation of the left eye and simultaneous extracellular multielectrode recording in the V1. **D.** Light flashes (yellow box) fail to evoke any responses. This period is "Light

blind" period (P7 and younger). Asterisk stands for spontaneous delta brush. **E-F.** Flashes of light trigger delta-brushes. This period is named "Light-evoked bursting" period (P8–11). **G-H.** Light flashes evoke only adult-like visual evoked potentials (VEP), but no delta brushes anymore. This period is called "Acuity" period (P12 and onward) (modified from Khazipov and Luhmann, 2006;Colonnese et al., 2010).

1.4 Intrinsic cellular resonance properties contribute to the synchrony oscillations.

Oscillatory activity requires temporal synchronization of neuronal assemblies and can be attributed to delays within the synaptic circuitry and/or certain intrinsic cellular properties (Buzsaki and Draguhn, 2004). Membrane resonance is a cellular property that particularly contributes to synchronization (Hutcheon and Yarom, 2000) and provides a mechanism for selecting synaptic inputs from presynaptic neurons with correspondingly tuned spike patterns (Izhikevich et al., 2003). Membrane resonance emerges from the interaction between passive membrane properties, which determine low-pass filter properties, and additional currents with a slow time constant that actively oppose the passive membrane potential changes, which add high-pass filter properties to the neuronal membrane (Hutcheon and Yarom, 2000).

In guinea-pig cortical neurons, about 50% of the cells showed spontaneous subthreshold oscillations. While sinusoidal current were injected to these cells, they expressed subthreshold resonance. Interestingly, both subthreshold oscillations and resonance had the same basic frequencies. Application of TTX significantly decreased the resonance strength while subthreshold oscillations were fully blocked by TTX. All these results suggested that there is a close association between the subthreshold oscillations and the resonance behaviour in neurons (Gutfreund et al., 1995). In trigeminal mesencephalic neurons expriments indicated that subthreshold oscillations also emerged from the voltage-dependent resonant properties. Similar with the previous study, in these oscillatory neurons, the frequency of subthreshold oscillations and the resonant frequency were within the same range. Furthermore,

low dose of 4-aminopyridine (< 100 μM) reduced the oscillations and blocked resonance in most neurons. TTX also decreased substantially the oscillations and resonance strength. Taken together, these results indicated that the same mechanisms underlied subthreshold oscillations and resonance and further suggested that the oscillations emerged from membrane resonance (Wu et al., 2001).

In addition, Lampl and Yarom found that the guinea-pig olivary neurons had spontaneous oscillations as well as resonance peak coincided at the same frequency band which suggested that the resonance behavior and the subthreshold oscillatory had a close relationship (**Fig. 4**). After application of Ni^{2+}, both subthreshold oscillations and resonance were abolished. These results suggested that the resonance behavior of individual neurons is the basic of the oscillatory behavior of the network. (Lampl and Yarom, 1997).

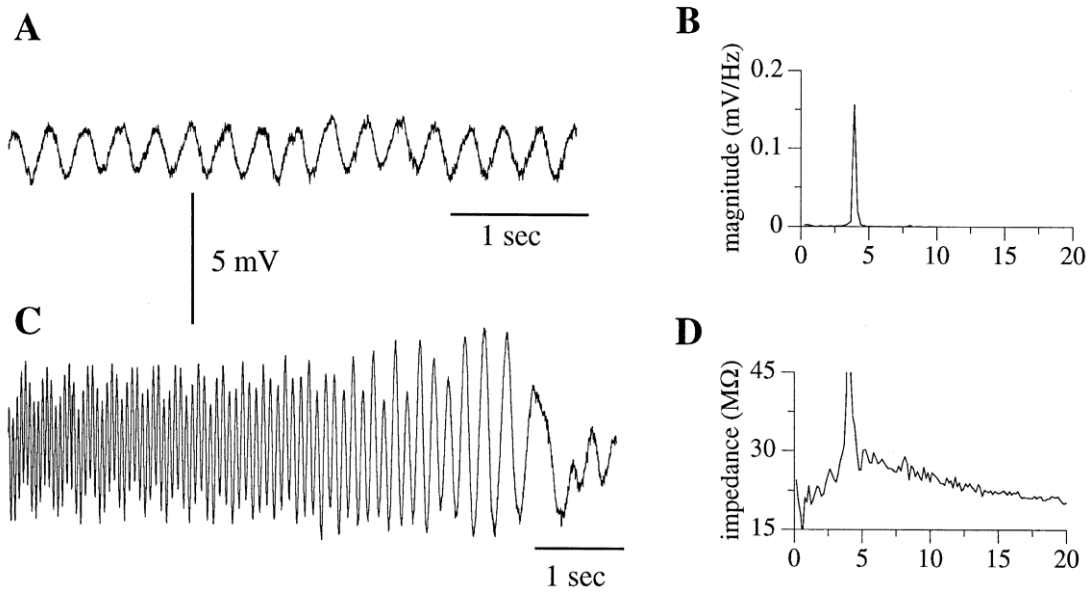

Fig. 4 Similar frequencies observed both in spontaneous oscillations and resonance behaviour.

A: The spontaneous oscillations recorded in the populations of olivary neurons in guinea-pig. **B:** The power spectrum of the oscillations as in A shows a sharp peak at a frequency of 3.9 Hz. **C:** A single olivary neuron to a ZAP input expressed resonant response. **D:** The impedance-frequency curve calculated from the same neuron as in C shows that a peak at a frequency similar as the frequency of oscillations. (modified from Lampl and Yarom, 1997).

1.5 Different cellular mechanisms contribute to the resonance

Subthreshold resonance arises from interactions of membrane resistance, capacitance and inductive elements in a parallel configuration. The passive membrane properties capacitance and resistance are determined by the surface of the plasma membrane and by leak conductances and establish the low-pass filtering characteristic innate to all neurons (Barrett and Crill, 1974). The inductive elements responsible for the generation of membrane resonance can be generated by voltage-dependent conductances with an activation kinetic that is larger than the membrane time constant (Hutcheon and Yarom, 2000). Thereby the add "high-pass" properties to the neuronal membrane, which is an important element of resonance (Hutcheon and Yarom, 2000). In particular I_h, persistent Na^+ currents (I_{NaP}), t-type Ca^{2+} and m-type K^+ currents have been suggested to underlie the inductive element of membrane resonance (Puil et al., 1994;Hutcheon et al., 1996;Pape and Driesang, 1998;Hu et al., 2002;Zemankovics et al., 2010).

I_h is mediated by hyperpolarization-activated cyclic nucleotide-gated (HCN) channels. HCN channels are nonselective ligand-gated cation channels in the plasma membranes of heart and brain cells. HCN channels are encoded by four genes (HCN1,2,3,4) and are widely expressed throughout the heart and central nervous system. I_h is a mixed cation (Na^+, K^+) current that reverses close to -20 mV and is activated by hyperpolarizations beyond -60 mV (Brown and Adams, 1980;Halliwell and Adams, 1982;Brown et al., 1990;Storm, 1990). I_h flows inward over its entire activation range and can be blocked by the I_h/HCN channel blocker ZD7288 (Hu et al., 2002;Wang et al., 2006;Zemankovics et al., 2010). It has been proved that I_h is critical for not only for oscillations, pacemaking, but also for the resonance in a variety of cell types, from cardiac pacemaker cells to thalamic neurons (Pape, 1996;Luthi and McCormick, 1998;Neuhoff et al., 2002). In rat neocortical neurons, about 60% of regular spiking (RS) and intrinsic bursting (IB) neurons showed resonance at resting membrane potentials. Their resonance frequencies were between

0.7 and 2.5 Hz near -70 mV and increased with hyperpolarization and decreased with depolarization (Hutcheon et al., 1996). What's more, bath applied Cs^+, a blocker of I_h, could abolish subthreshold resonance. Therefore, it was concluded that I_h generated the subthershold resonance in these cells. Similarly, in rat hippocampal CA1 pyramidal neurons, resonance frequency was observed from 2 to 7 Hz. Interestingly, the blocker of I_h (ZD7288) abolished the resonance only at hyperpolarized potentials which suggested that 'H-resonance' generated by the h-current in hyperpolarized cells (Hu et al., 2002). I_h is also expressed in interneurons (Aponte et al., 2006;Zemankovics et al., 2010) and has been shown to be essential for the generation of subthreshold resonance in different classes of adult hippocampal interneurons (Zemankovics et al., 2010).

The T-type Ca^{2+} channel is a type of voltage-gated calcium channel, which is prominently expressed in a variety of brain regions, such as neocortex, hippocampus and thalamus (Puil et al., 1994;Huguenard, 1996;Ertel and Ertel, 1997). "T" stands for transient referring to the length of activation. T-Type Ca^{2+} channels are low-voltage-activated (LVA) Ca^{2+} channels: they start to open when cells depolarize to between -60 and -40 mV, at much more negative potentials than other voltage-gated Ca^{2+} channels. They open and inactivate rapidly, but their most remarkable kinetic property is that they close (deactivate) much more slowly (10-100 fold) than other voltage -gated Ca^{2+} channels. T-type Ca^{2+} currents can be relatively selective blocked by Ni^{2+} (Ertel and Ertel, 1997). In thalamic neurons, most neurons displayed resonance and their resonance frequency were between 2-4 Hz near the resting potentials. Application of Ni^{2+} (0.5-1 mM) reduced the low frequency resonance, which suggested that the low threshold Ca^{2+} current contributed to the generation of low frequency resonant behavior of thalamus neurons (Puil et al., 1994;Hutcheon et al., 1994). In addition, in olivary neurons of guinea-pig, the subthreshold resonance was almost completely abolished in the presence of 1 mM of Ni^{2+} (Lampl and Yarom, 1997). All these results demonstrate that t-type Ca^{2+} channels mediate subthreshold resonance in these neuronal populations.

The persistent Na^+ current (I_{NaP}) is a threshold current which have been found in neocortical and hippocampal pyramidal neurons (French and Gage, 1985;Stafstrom et al., 1985), hippocampal and cerebellar interneurons (Solinas et al., 2007;Boehlen et al., 2011), and many other neurons in different brain regions (Crill, 1996). I_{NaP} was activated positive to -65 mV and could be blocked by tetrodoxin (TTX, 1 μM). Persistent Na^+ currents have been shown to contribute importantly to intrinsic oscillations of some central neurons (Klink and Alonso, 1993;Gutfreund et al., 1995;Hutcheon et al., 1996;Pape and Driesang, 1998;Hu et al., 2002), in cerebellar interneurons (Solinas et al., 2007) and hippocampal stratum radiatum interneurons (Boehlen et al., 2011). In rat neocortex, regular spiking (RS) and intrinsic bursting (IB) neurons exhibited resonance at resting membrane potentials. They suggested that I_h produced subthreshold resonance to these cells. However, application of TTX greatly reduced resonance at depolarized potential, which suggesting that I_{NaP} amplified resonance at depolarization state (Hutcheon et al., 1996). Similarly, subthreshold resonance of rat subicular pyramidal neurons could also be suppressed in the presence of TTX at depolarize potentials (Wang et al., 2006). What's more, in rat hippocampal pyramidal cells, the theta frequencies resonance could also be diminished by application of TTX at depolarized, but not hyperpolarized membrane potentials (Hu et al., 2002). Taking together, all these results suggested that I_{NaP} normally amplified resonance when these cells in depolarization state.

Last but not least, m-type K^+ currents (I_M) also suggested to be involved in subthreshold resonance (Hu et al., 2002;Hu et al., 2009;Heys et al., 2010). I_M is a type of noninactivating potassium current first discovered in bullfrog sympathetic ganglion cells (Brown and Adams, 1980). The M-channels are voltage-gated K^+ channels and encoded by the KCNQ gene family (Wang et al., 1998), which comprises five genes in mammals (Jentsch, 2000). M current activated positive to -65 mV and was blocked by the M/KCNQ channel blocker XE991 (Hu et al., 2002;Hu et al., 2009). The M-channels are important in raising the threshold for firing an action potential. There are also some researches suggest that M-currents

regulate the excitability of a variety of neurons (Brown and Adams, 1980;Halliwell and Adams, 1982). Furthermore, I_M is also involved in subthreshold resonance. For example, in rat hippocampal CA1 pyramidal neurons, resonance phenomenon was observed both at depolarization and hyperpolarztion potentials. Interestingly, application of XE991 (10 μM) or TTX (1 μM) could only blocked the resonance at depolarized but not at hyperpolarized potential, suggesting that 'M-resonance' generated by the M-current and persistent Na^+ current in depolarized cells (Hu et al., 2002). Similarly, in layer II stellate cells of meidial entorhinal cortex, M-current generated membrane potential resonance at depolarized, but not hyperpolarize membrane potentials (Heys et al., 2010). Moreover, Hu and his colleague found theta resonance in hippocampal CA1 pyramidal neurons also caused by M-current (Hu et al., 2009). All these results show that M-current contribute to subthreshold resonance in these neurons at depolarized membrane potentials.

In summary, all these studies show that I_h, t-type Ca^{2+}, persistent Na^+ currents and m-type K^+ currents underlie the inductive element of membrane resonance in different brain regions (Puil et al., 1994;Hutcheon et al., 1996;Pape and Driesang, 1998;Hu et al., 2002;Zemankovics et al., 2010).

1.6 Neuronal resonance in brain regions

Neuronal resonance has been observed in a variety of neurons located in the sensorimotor cortex (Hutcheon et al., 1996), the entorhinal cortex (Haas and White, 2002;Erchova et al., 2004), the hippocampus (Leung and Yu, 1998;Hu et al., 2002;Zemankovics et al., 2010), the amygdala (Pape and Driesang, 1998), the cerebellum (Solinas et al., 2007), the thalamus (Puil et al., 1994) and other brain regions (van Brederode and Berger, 2011). In rat sensorimotor cortex, approximately 60% of regular spiking (RS) and intrinsic bursting (IB) neurons showed subthreshold resonance at their resting membrane potentials and their resonance frequency were between 0.7 and 2.5 Hz (Hutcheon et al., 1996). In rat entorhinal cortex, Erchova and her colleagues also observed subthreshold resonance in the range of 5-15 Hz in layer

II stellate cells, but suprisingly not in layer III cells (Erchova et al., 2004). Moreover, hippocampal CA1 pyramidal neurons also showed subthreshold resonance in theta band (Leung and Yu, 1998;Hu et al., 2002). GABAergic interneurons express very heterogeneous resonance behaviors. In hippocampal fast-spiking interneurons rather high resonance frequencies up to 50 Hz were observed (Pike et al., 2000), whereas the resonance frequency in other hippocampal interneurons in the stratum oriens was between 2 and 8 Hz, mainly covering the theta range(Pike et al., 2000;Zemankovics et al., 2010;Boehlen et al., 2011). However, on some classes of hippocampal interneurons subthreshold resonance is absent (Zemankovics et al., 2010;Anderson et al., 2011). In the basolateral amygdaloid complex of the guinea pig, spiny neurons exhibit resonance at about 2 Hz (Pape and Driesang, 1998). In the cerebellum, the inhibitory Golgi cells also display resonance in the delta to theta range (Solinas et al., 2007). In thalamic neurons of rat, most neurons displayed resonance and their resonance frequency were between 2-4 Hz near the resting potentials. Interestingly, the other wide band (12-26 Hz) of peak resonant frequencies was observed at depolarized levels (Puil et al., 1994). Recently, GAD67 positive interneurons in the nucleus Roller have been demonstrated to express a weak resonance in the delta band (van Brederode and Berger, 2011).

1.7 Different locations, morphologies and functions of neuronal populations in cerebral cortex

Cajal-Retzius (CR) cells are among the first neuronal classes generated in the embryonic telencephalon. These transient populations of early-born glutamatergic cells are mainly found in the marginal zone of the mammalian cerebral cortex (Soriano and del Rio, 2005). These cells locate directly below the pial surface and have ovoid somata and one single root-like dendrite (**Fig. 5A**). Moreover, CR cells cover the whole cortical surface before emergence of the cortical plate. There are two different subtypes of CR cells distinguished by their origins, onset of appearance, migration routes, destination and expression of molecular markers. CR cells originate

from at least three distinct focal areas: the cortical hem in the caudomedial wall of the telencephalic vesicles, the pallial septum (PS), and the ventral pallium (VP) (Meyer et al., 2002;Takiguchi-Hayashi et al., 2004;Bielle et al., 2005). During the early development of the cerebral cortex, CR cells produce substantial amounts of reelin, which play an important role in the organization of cortical layers formation (Bar et al., 2000). Furthermore, knocking out the Reln gene resulted in the abnormal cortical formation and disorganized cortical plate. Therefore, the diversity and distinct locations of CR cells have been suggested to be critical for the cortical development (Griveau et al., 2010).

Subplate cells are also among the first generated neurons in the mammalian cerebral cortex. This transient population of neurons is located between the intermediate zone and the cortical plate, which will disappear during postnatal development (Kanold, 2009;Luhmann et al., 2009). These cells have a large variety of morphologies (**Fig. 5B**). Subplate cells represent a heterogeneous population of multipolar or bipolar cells with a horizontal or inverted vertical orientation (Luhmann et al., 2000;Hanganu et al., 2001;Kanold and Luhmann, 2010). Three subplate subpopulations were distinguished by the various novel markers, which have the distinct projection profiles (Grant et al., 2012). These neurons play a crucial role in the regulation of the early cortical development, the structural and functional organization of the cerebral cortex, and the neocortical plasticity. For example, in the developing neocortical network, the subplate cells can balance excitation and inhibition by regulating the maturation of GABAergic synaptic transmission (Kanold and Shatz, 2006). Moreover, they receive a transient synaptic input from “waiting” thalamic axons (Lund and Mustari, 1977;Rakic, 1977;Rakic, 1983) and extend the axons to corticofugal pathway and have been suggested to guide thalamocortical axons (Allendoerfer and Shatz, 1994;Molnar et al., 1998). Then, subplate cells are proposed to be an active element amplifier of neuronal activity from thalamus or other cortical areas (Luhmann et al., 2009). Accordingly, early deletion of subplate neurons in kitten visual cortex prevents the segregation of thalamocortical axons within layer IV and destroys the formation of ocular

dominance columns (Ghosh and Shatz, 1992;Kanold et al., 2003).

Pyramidal neurons are located in cerebral cortex and other brain regions (hippocampus and amygdala). During the early postnatal development of neonatal cerebral cortex, a pool of postmitotic pyramidal precursors has been identified in the dorsomedial (dm) part of the ventricular/subventricular zone (VZ/SVZ). These unmatured cells travel through the white matter and migrate into the medial limbic cortex (Zgraggen et al., 2012). In the adult cerebral cortex, these cells are mainly located at the layer II/III and layer V. These cells have classical morphology (**Fig. 5C**). The neuron has the triangular shaped soma, a single axon, a large apical dendrite, multiple basal dendrites, and the presence of dendritic spines (Megias et al., 2001). However, the specific structures of the pyramidal cells vary in different brain areas where these cells have various functions. In the sensory cortex, the layer II/III pyramidal cells participate in tactile information processing. Furthermore, reliable experience-dependent plasticity can be found in these cells (Diamond et al., 1994;Huang et al., 1998;Fox, 2002;Feldmeyer et al., 2005). Finally, these cells have been proposed to have memory storage capacity (Diamond et al., 1994;GoldmanRakic, 1996;Harris et al., 2002). The layer Va pyramidal cells has been suggested to participate in the intracortical processing of sensory information (Schubert et al., 2006). In the barrel cortex, intrinsically burst-spiking firing pattern of pyramidal neurons were suggested to be the candidates for multi-whisker integration (de Kock et al., 2007). The largest pyramidal cells in the central nervous system are named Betz cells (Braak and Braak, 1976). They are pyramidal neurons located in the layer of primary motor cortex (Braak and Braak, 1976). These corticospinal neurons have been reported to contribute to the discrete voluntary skilled movements, such as precise movement of the fingers and toes (Lemon, 2008).

Interneurons are rich in the cerebral cortex. In adult, there are two main classes of cortical GABAergic interneurons: petisomatic and dendritic inhibitory cells. Different kinds of the dendritic inhibitory interneurons have been reported in the neocotex (Markram et al., 2004). They are Martinotti cells, double bouquet cells, biplolar cells, bitufted cells and neurogliaform cells. Although there are many

different subtypes of interneurons, these cells have comparable structures (**Fig. 5D**). Both dendrites and axon are cable-like and the long extension from the soma. Moreover, they have more dendrites than pyramidal cells, which contribute to the communications with other neurons (Dumitriu et al., 2007). These neurons project to different regions of the pyramidal cell, including the dendrites, soma and axon and compose different functional circuits. Different morphological and physiological properties of interneurons have various functions. However, they have functions in common. For example, these neurons maintain physiological activity levels and keep the balance between the excitation and inhibition (Ziskind-Conhaim, 2013). Some interneurons play a crucial role in the generation of network oscillations and modify the other principal neurons activity (Mann and Paulsen, 2007). Interaction between interneurons and other excitatory neurons have been proposed to be the mechanisms of gamma oscillation (Buzsaki and Wang, 2012). Furthermore, these neurons have been suggested to be involved in the cortical computations., such as working memory and decision-making in the neocortex (Machens et al., 2005).

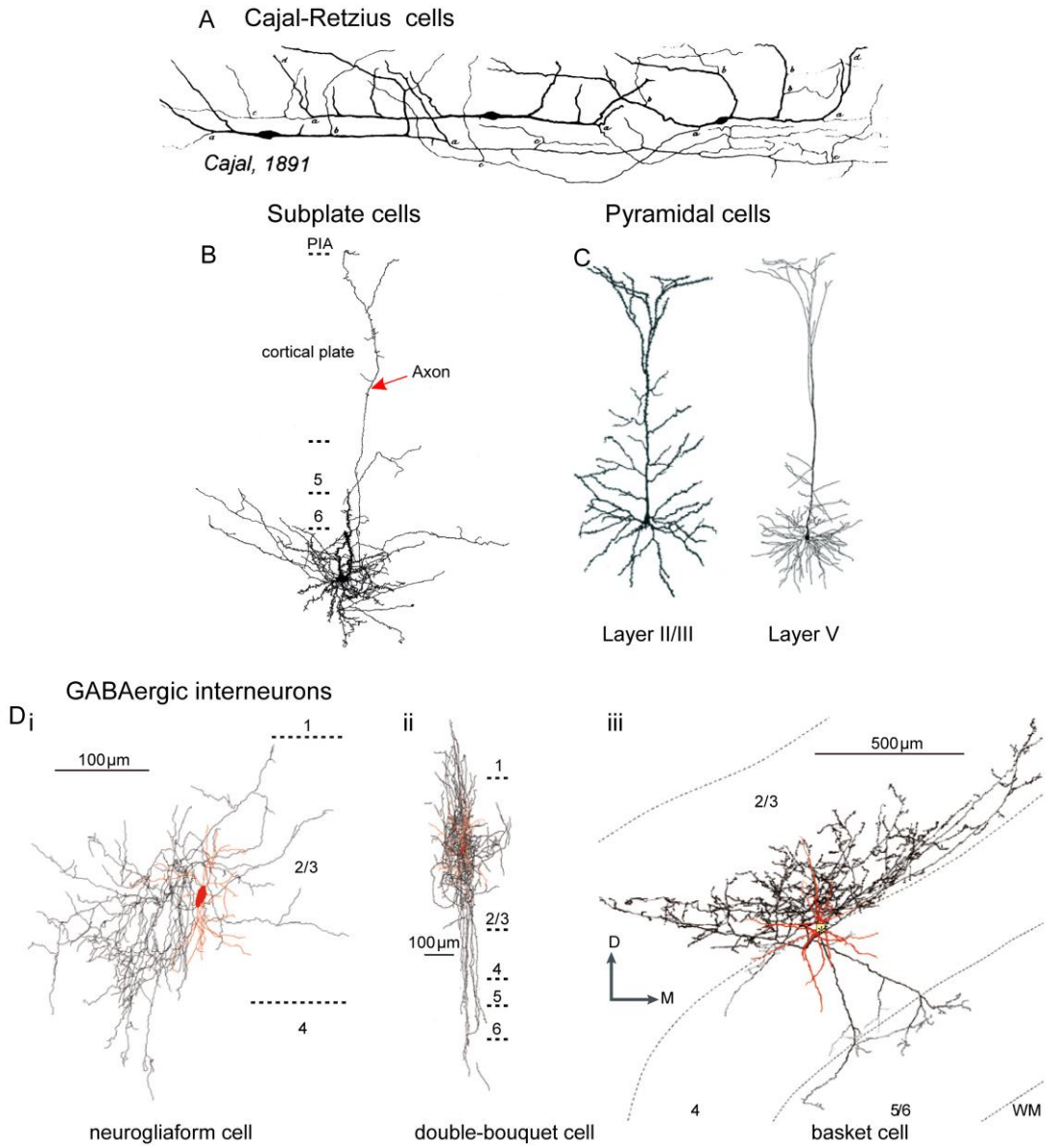

Fig. 5 Different locations and morphologies of cortical neurons.

A: Cajal described in 1891 slender horizontal bipolar cells in the developing marginal zone of lagomorphs. Note that these cells locate directly below the pial surface and have ovoid somata and one single root-like dendrite. **B:** An example of a subplate neuron in newborn rat visual cortex that has been filled with biocytin. Note that the cell's axon extends vertically into the cortical layers, while the dendrites cluster around the soma locate at the base of layer 6. The red arrow indicates axon. **C:** The examples of pyramidal neurons from layer II/III and V in rat cerebral cortex. Both neurons have basal and apical dendrites and an apical tuft. However, considerable differences could be observed between these two shown. Note that layer V pyramidal neurons have longer apical dendrites and fewer oblique apical dendrites than layer II/III pyramidal neurons. **D:** The structures of dense plexus of highly branched axons and dendrites in different interneurons from different layers. **(i)** A neurogliaform cell

from the rat somatosensory cortex. Black stands for the soma and dendrites, while red is axon. **(ii)** A double-bouquet cell from the cat primary visual cortex. The soma and dendrites are shown in red and the axon is shown in black. Note the characteristic horsetail-like axonal distribution. **(iii)** Morphological characteristics of a layer-3 large basket cell from the cat primary visual cortex. Red indicates the soma and dendrites, while black shows the axon. Note that the axon arborized profusely in the lower half of layer 3 and had a lateral extent of 1.1 mm from the parent soma. (modified from Meyer et al., 1999;Ascoli et al., 2008;Spruston, 2008;Friedlander and Torres-Reveron, 2009)

1.8 Aims of the thesis

In the immature neocortex oscillatory activity patterns in different frequency domains ranging from low delta range (0.5-4 Hz) to gamma range (30-100 Hz) are observed already in the first postnatal week (Engel et al., 2001;Dupont et al., 2006;Yang et al., 2009;Brockmann et al., 2011;Minlebaev et al., 2011;Yang et al., 2012). However, the neuronal processes underlying these neocortical oscillations remain unresolved at the time I started my work on this project. Further, no information was available on the resonance properties of cortical neurons during the first postnatal week and the underlying mechanisms

In this thesis, I therefore address the question of resonance properties and mechanisms of different neuronal populations in the immature mouse neocortex. I characterized the impedance profile of Cajal-Retzius cells, cortical plate neurons, layer II/III and layer V pyramidal neurons, subplate cells as well as GABAergic interneurons in slices of P0-P13 mice, using sinusoidal current injections under whole-cell patch-clamp conditions. To identify the membrane currents underlying the observed resonance I performed pharmacological experiments, which unraveled that hyperpolarization-activated cation currents (I_h), t-type Ca^{2+} currents and persistent Na^+ currents contribute to the membrane resonance in immature neocortical neurons. I propose that membrane resonance of immature neurons may contribute to the generation of slow oscillatory activity pattern in the immature

neocortex and enhance the temporal precision of synaptic integration in developing cortical neurons. Part results were already published (Sun et al., 2012).

2 Materials and Methods

2.1 Slice preparation

All experiments were performed in accordance with EU directive 86/609/EEC for the use of animals in research and approved by the local ethical committee (Landesuntersuchungsanstalt RLP, Koblenz, Germany). All efforts were made to reduce the number of experimental animals and their suffering. Coronal and tangential slices were prepared from brains of P0 to P2 , P5 to P7 C57Bl/6 mice and P6 to P13 pups from heterozygous GAD67-GFP knock in mice (Tamamaki et al., 2003). Newborn GAD67-GFP knock in pups were phenotyped on P1-P3 by examining the fluorescence of the brain through the thin skull of the newborn using a LED light source with adequate filter sets (Model GFsP-5; BLS, Budapest).

On the experimental day mice pups were deeply anesthetized by hypothermia, decapitated, and the brains were removed and immersed in ice-cold (<4 °C) artificial cerebrospinal fluid (ACSF, composition see below). Coronal slices (400 µm thick) including the somatosensory cortex were prepared using a vibratome (HR2, Sigmann Elektronik, Hüffenhardt, Germany) and separated into two hemispheres. Tangential slices were prepared as described in detail in a previous report (Achilles et al., 2007). Isolated hemispheres were glued to the bottom of a petridish, leptomeninges were carefully removed with a fine forceps, tangential slices with a maximal thickness of ~600 µm were cut by hand with a razor blade and were attached to fine tissue paper. All preparations were allowed to equilibrate in oxygenated ACSF at room temperature for 1 h before they were transferred to the submerged-type recording chamber.

2.2 Electrophysiological recordings

Recordings were obtained at 29 ± 2 °C from visually identified Cajal-Retzius

cells in tangential slices (Achilles et al., 2007) and from cortical plate, layer II/III and layer V pyramidal neurons as well as subplate cells in coronal slices (Luhmann et al., 2000;Hanganu et al., 2001;Hirsch and Luhmann, 2008) and GABAergic interneurons from GAD67-GFP knock in mice, according to protocols published before (Sava et al., 2010). Using an upright microscope (Axioskop 2 FS plus; Zeiss, Jena, Germany) equipped with epifluorescence and infrared differential interference contrast (DIC) optics, and a video system (Hamamatsu Photonics). Pictures of cells were digitized by a frame grabber card (Screen Machine II; Fast, Munich, Germany) and stored on the computer. For imaging of GFP fluorescent neurons an Hg-Arch lamp and an appropriate filter set (λ_{ex} 530-550nm, λ_{em} 590 nm, $\lambda_{Dichr.}$ 570 nm) was used. Intensity and duration of fluorescent illumination were minimized to prevent cell damage. Recording electrodes were pulled from borosilicate tubes (GC200F; Science Products, Hofheim, Germany), using a vertical puller (PP430, Narishige) and were filled with (in mM): 80 K-gluconate, 44 KCl, 2 $MgCl_2$, 1 $CaCl_2$, 11 EGTA, 10 K-Hepes, 2 Na_2-ATP, 0.5 Na-GTP (pH adjusted to pH 7.4 with KOH and osmolarity to 306±2 mOsm with sucrose). Electrode resistance was 4-5 MOhm. Recordings were performed using a conventional patch-clamp amplifier (EPC-7; List, Darmstadt, Germany). Signals were amplified and low-pass-filtered at 3 kHz, digitized online with an AD/DA-board (ITC-16; Heka, Lambrecht, Germany), and analyzed off-line using WinTida software (Heka). Seal resistance was determined immediately before the seal was opened. The average seal resistance of Cajal-Retzius cells was 5.3 ± 0.4 GOhm (n=58), of supragranular neurons 5.5 ± 0.4 GOhm (n=67), of layer V pyramidal neurons 4.4 ± 0.3 GOhm (n=95), of subplate cells 5.9 ± 0.4 GOhm (n=56), and of GABAergic interneurons 4.6 ± 0.3 GΩ (n=86). Resting membrane potential was determined immediately after the whole-cell condition was established. For the determination of input resistance and membrane time constant, hyperpolarizing current pulses of 10 pA or 20 pA amplitude were applied from a holding potential of -66 mV. The membrane time constant (τ) was calculated by fitting a monoexponential function of the type a + b × exp (time/c) to the induced potential deflection. Active membrane properties were assessed by recording responses to a

series of hyperpolarizing and depolarizing current pulses from a holding potential of -66 mV. Spike amplitude was measured from the baseline to the peak and spike width was determined at half-maximal amplitude. Spike frequencies were determined with proper settings of the Minianalysis Software 4.3.3 (Synaptosoft, Leonia, NJ). All potentials were corrected post-hoc for a liquid junction potential of 6 mV. The measured resting membrane potential was corrected post-hoc according to the formula delivered by (Tyzio et al., 2003), to correct voltage errors caused by the short circuit via the seal conductance. For experiments in which the seal resistance was not determined the average seal resistance was used.

2.3 Identification of cells

Cells in the neocortex were classified according to their laminar position, morphology of the somata, ramification, and orientation of the proximal dendrites (Luhmann et al., 2000). For a more detailed morphological analysis and verification of the DIC image-based identification, 0.5 % biocytin (Sigma, Steinheim, Gemany) was added to the pipette solution, which was processed according to published protocols (Achilles et al., 2007). In brief, slices were fixed in 4% paraformaldehyde overnight, stained with streptavidin coupled Cy-3 (Dianova) fluorophore, C57Bl/6 mice slices embedded in fluoromount (Sigma). Fluorescence was excited with the 568 nm line of a Kr / Ar laser (Laser Physics, Malpas, Uk). For GAD-67 GFP positive interneurons, incubated overnight at RT with a rabbit anti GFP antibody (1:500, Invitrogen, Karlsruhe, Germany), and subsequently with a donkey anti-rabbit IgG secondary antibody conjugated with Dylight 488 (1:100; Dianova). Fluorescence was investigated with a Nipkow spinning disk confocal system (Visitech, Sunderland, UK) using 488/568 nm lines of a Kr/Ar laser (Laser Physics, Malpas, UK).

Horizontal bipolar cells located directly below the pial surface with ovoid somata and one single root-like dendrite were classified as Cajal-Retzius cells (**Fig. 6A**). Vertically oriented neurons located in the upper cortical plate of slices from

P0-P2 animals with a bifurcated dendrite clearly extending towards the cortical surface were classified as cortical plate pyramidal neurons (**Fig. 6B**). In P5-P7 mouse cortex the cortical plate disappears and in coronal slices layer II/III pyramidal neurons with a short apical dendrite can be identified below the pial surface. Layer V pyramidal neurons were identified according to their laminar location, their large somata, and their prominent apical dendrite ascending to the pial surface (**Fig. 6C**). A heterogeneous population of multipolar or bipolar cells with a horizontal or inverted vertical orientation that were located in a small layer immediately above the white matter (**Fig. 6D**) were classified as subplate cells (Luhmann et al., 2000;Hanganu et al., 2001;Kanold and Luhmann, 2010). For GAD-67 GFP positive interneurons, only neurons that showed a clear consistency in location, soma shape and morphology of distal neurites between the fluorescence and DIC image were selected for investigation (**Fig. 17A**).

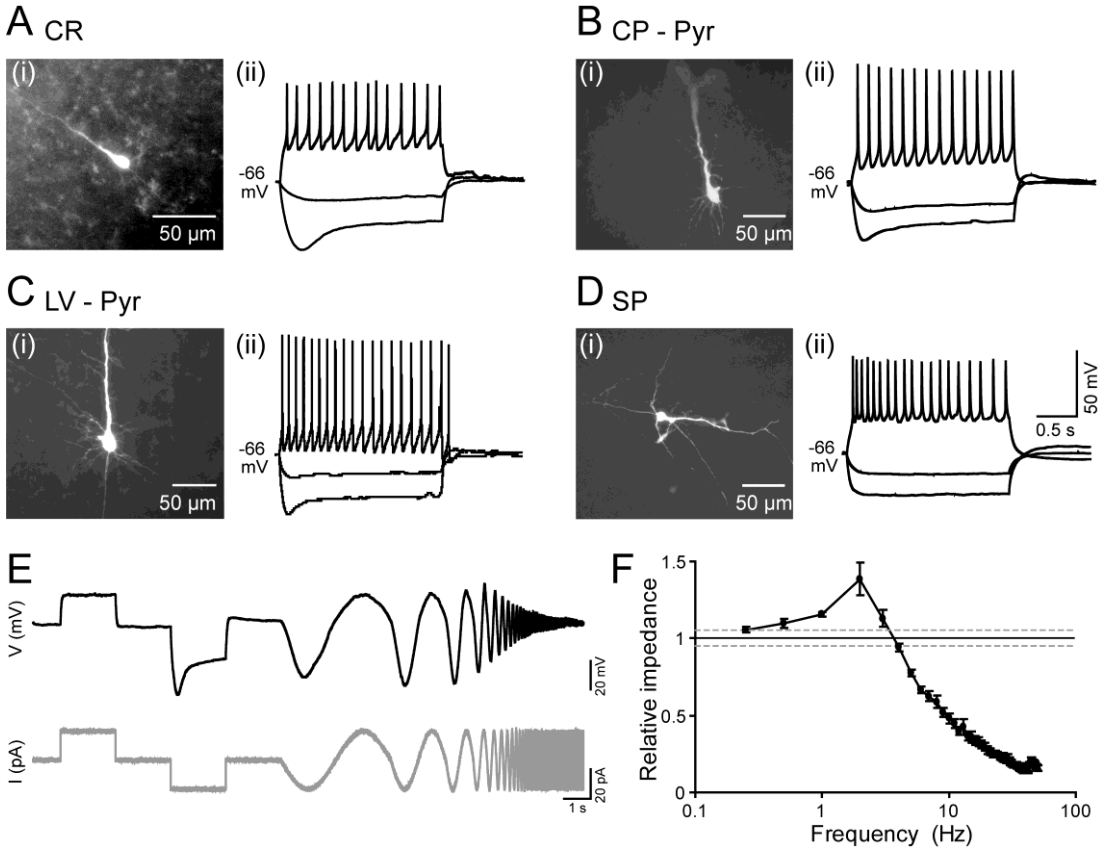

Fig. 6 Identification of typical neuronal cell populations in the immature cerebral cortex and analyses of intrinsic resonance properties.

A: Photomicrograph of a biocytin-stained Cajal-Retzius (CR) cell in a tangential slice of a P2 mouse **(i)** and characteristic response pattern of this cell upon injection of de- and hyperpolarizing currents **(ii).** Note the typical root-like morphology and the prominent voltage-sag. **B:** Photomicrograph and typical electrophysiological properties of a cortical plate pyramidal neuron (CP-Pyr) in a coronal slice from a P1 mouse. Note the typical bifurcated apical dendrite without further ramification. **C:** Photomicrograph and typical electrophysiological properties of a LV pyramidal neuron (LV-Pyr) in a P6 mouse coronal slice. Note the dense basal dendrites, the long apical dendrite and the mature discharge pattern with large amplitude action potentials. **D:** Photomicrograph and electrophysiological properties of a subplate neuron (SP) in a P0 mouse coronal slice. Note the fusiform soma and the horizontal bitufted dendritic tree. **E:** Protocol used to analyze neuronal resonance. After characterization of steady-state resistance by injection of de- and hyperpolarizing currents the frequency dependent impedance was tested by a sinusoidal current protocol with constant amplitude and increasing frequency (0.25-200 Hz). The impedance was calculated from voltage response and normalized to the steady-state resistance. **F:** Relative impedance profile of the recording shown in E. Datapoints represent mean ± SEM. The dashed lines represent SD of the steady-state impedance in 6 repetitions. (from Sun et al., 2012).

2.4 Characterization of electrical resonance

To characterize the intrinsic resonance properties, we used three to ten sweeps of a sinusoidal current protocol with constant amplitude and increasing frequency (0-200 Hz during 20 s) under current-clamp conditions (**Fig. 6E**). The sinusoidal current protocol consisted of distinct frequencies lasting one cycle. The amplitude of the sinusoidal current was adjusted to keep the voltage response below action potential threshold. Resonance properties were tested at holding potentials close to -66 and -86 mV, which were manually adjusted by steady current injection. To analyze the resonance, the impedance at a given frequency (Z_f) was calculated from single sweeps by dividing voltage responses by injected currents. For impedance spectra Z_f was normalized to the steady state impedance (Z_0) calculated from the steady state current injection (**Fig. 6F**). The optimal resonance frequency (f_{res}) was

determined at the maximal impedance (Q) in the impedance spectrum. Neurons, in which Q was not significantly (Students t-test, $P \geq 0.05$) different from Z_0 or in which f_{res} was below 0.5 Hz, were considered as non-resonant neurons. The cutoff frequency was defined as the highest frequency at which $Z_f \geq$ - 3dB.

2.5 Solution and Drugs

The ACSF solution used for preparation, storage and recording contained (in mM): 126 NaCl, 26 $NaHCO_3$, 1.25 NaH_2PO_4, 2.5 KCl, 2 $CaCl_2$, 1 $MgCl_2$ and 10 glucose, pH 7.4 after equilibration with 95% O_2 and 5% CO_2, 310 mOsm. ZD7288 (4-Ethylphenylamino-1,2-dimethyl-6-methylaminopyrimidin chloride, Tocris, Eching, Germany) was used from a 50 mM stock solution in distilled water, Cs^+ (Sigma) from a 2.5 M stock solution in distilled water, Ni^{2+} (AppliChem, Darmstadt, Germany) from a 2 M stock solution in distilled water and tetrodotoxin (TTX, Sigma) from a 1 mM stock solution in distilled water.

2.6 Statistics

All values are given as mean ± standard error of the mean (SEM). For statistical comparisons of paired and unpaired datasets sign-test and Mann-Whitney U-test, respectively, were used (Systat 11 and SPSS 13.0, IBM). Incidence rates were compared with Fisher exact test (Systat 11).

3. Results

3.1 Properties and mechanisms of subthreshold resonance in Cajal-Retzius cells

"Whole-cell patch-clamp recordings were obtained from 30 P0-P2 and 31 P5-P7 Cajal-Retzius cells in mice tangential slices. Their resting membrane potential was -52.3 ± 0.9 mV and -54 ± 0.7 mV, respectively. Their membrane time constants as well as other passive and active membrane properties (**Table 1**) are in agreement with previous studies (Kilb and Luhmann, 2001;Radnikow et al., 2002).

	Passive membrane propertie				Action potential properties		
	E_m (mV)	E_m^0 (mV)	R_{input} (GΩ)	C_{input} (pF)	Threshold (mV)	Amplitude (mV)	$d_{1/2}$ (ms)
Cajal–Retzius							
P0–P2	-52.3 ± 0.9 (n= 30)	-78 ± 3.5 (n= 30)	1.95 ± 0.14 (n= 30)	46.0 ± 1.6 (n= 30)	-37.1 ± 0.9 (n= 28)	37.9 ± 1.3 (n= 28)	3.5 ± 0.3 (n= 28)
P5–P7	-54 ± 0.7 (n= 31)	-82.3 ± 3.6 (n= 31)	2.06 ± 0.13 (n= 31)	44.1 ± 1.7 (n= 31)	-39.9 ± 0.6 (n= 31)	47.9 ± 1.1 (n= 31)	2.0 ± 0.1 (n= 31)
LII/III pyramidal							
P0–P2	-53.2 ± 3.1 (n= 15)	-63.3 ± 4.3 (n= 15)	1.38 ± 0.14 (n= 15)	48.6 ± 5.2 (n= 15)	-38.5 ± 0.5 (n= 15)	43.1 ± 2.4 (n= 15)	6.2 ± 0.4 (n= 15)
P5–P7	-62.2 ± 0.8 (n= 60)	-75.7 ± 1.7 (n= 60)	1.25 ± 0.06 (n= 60)	77.1 ± 3.6 (n= 60)	-39.0 ± 0.5 (n= 60)	56.5 ± 1.0 (n= 60)	2.9 ± 0.1 (n= 60)
LV pyramidal							
P0–P2	-56.6 ± 1.4 (n= 16)	-72.5 ± 4.2 (n= 16)	1.21 ± 0.11 (n= 16)	74.0 ± 4.6 (n= 16)	-40.6 ± 0.7 (n= 16)	58.7 ± 2.2 (n= 16)	6.0 ± 0.4 (n= 16)
P5–P7	-64.6 ± 0.5 (n= 87)	67.9 ± 1 (n= 87)	0.49 ± 0.03 (n= 87)	127.1 ± 5.5 (n= 87)	-41.7 ± 0.4 (n= 87)	71.9 ± 0.9 (n= 87)	2.2 ± 0.1 (n= 87)
Subplate							
P0–P2	-53.8 ± 0.8 (n= 45)	-73.4 ± 4 (n= 45)	1.60 ± 0.10 (n= 45)	70.4 ± 3.8 (n= 45)	-38.6 ± 0.6 (n= 45)	52.5 ± 1.4 (n= 45)	3.8 ± 0.1 (n= 45)
P5–P7	-57 ± 1.8 (n= 14)	-68.8 ± 3.3 (n= 14)	1.33 ± 0.17 (n= 14)	90.5 ± 11.3 (n= 14)	-36.7 ± 5.3 (n= 14)	61.2 ± 2.9 (n= 14)	2.9 ± 0.3 (n= 14)
GABAergic							
P6–P9	-64.4 ± 1.0 (n= 56)	-73.3 ± 1.4 (n= 56)	0.96 ± 0.08 (n= 56)	71.3 ± 5.1 (n= 56)	-42.4 ± 0.4 (n= 56)	63.4 ± 1.4 (n= 56)	2.1 ± 0.1 (n= 56)
P10–P13	-67.9 ± 1.2 (n= 41)	-73.0 ± 1.2 (n= 41)	0.48 ± 0.05 (n= 41)	101.9 ± 7.8 (n= 41)	-40.6 ± 0.5 (n=41)	66.3 ± 1.2 (n= 41)	1.5 ± 0.1 (n= 41)

Table. 1 Active and passive membrane properties of the investigated neuronal cell populations at different postnatal ages.

E_m is the measured resting membrane potential; E_m^0, estimated resting membrane potential after correction of short circuit effects via the seal conductance according to the formula delivered by Tyzio et al. (2003); R_{input}, input resistance; C_{input}, input capacitance; $d_{1/2}$ is action potential duration at half-maximal amplitude.

All Cajal-Retzius cells from both P0-P2 and P5-P7 cortices displayed a clear subthreshold resonance (**Fig. 7A, B**). The average resonance frequency at P0-P2 was 2.4 ± 0.1 Hz (n=30) and significantly (U-test, $U_{(58)}$ = 322.5, Z = -1.984, P = 0.047) increased to 2.9 ± 0.2 Hz (n=30) at P5-P7 (**Fig. 7Ci**). Resonance strength also significantly (U-test, $U_{(58)}$ = 311, Z = -2.055, P = 0.040) increased from 1.44 ± 0.04 to 1.57 ± 0.05 (**Fig. 7Cii**), and the cutoff frequency significantly (U-test, $U_{(58)}$ = 222,5 Z = -3.372, P < 0.001) increased from 10.3 ± 0.9 to 15 ± 1.1 Hz. In both age groups the resonance strength was considerably attenuated after the holding potential was shifted to -86 mV. Statistical analyses revealed that the resonance strength was significantly (U-tests; $U_{(50)}$ = 112, Z = -4.038, P < 0.001,and $U_{(49)}$ = 72, Z = -4.651, P < 0.001, respectively) reduced to 1.22 ± 0.02 (n=22) in P0-P2 and to 1.24 ± 0.02 (n=21) in P5-P7 Cajal-Retzius cells, while in both age groups the resonance frequency was not significantly affected by the hyperpolarized holding potential (**Fig. 7C**). The cutoff frequency was unaffected by hyperpolarization in both P0-P2 (10.6 ± 0.6 Hz, n=22) and P5-P7 (14 ± 1.2 Hz, n=21) Cajal-Retzius cells.

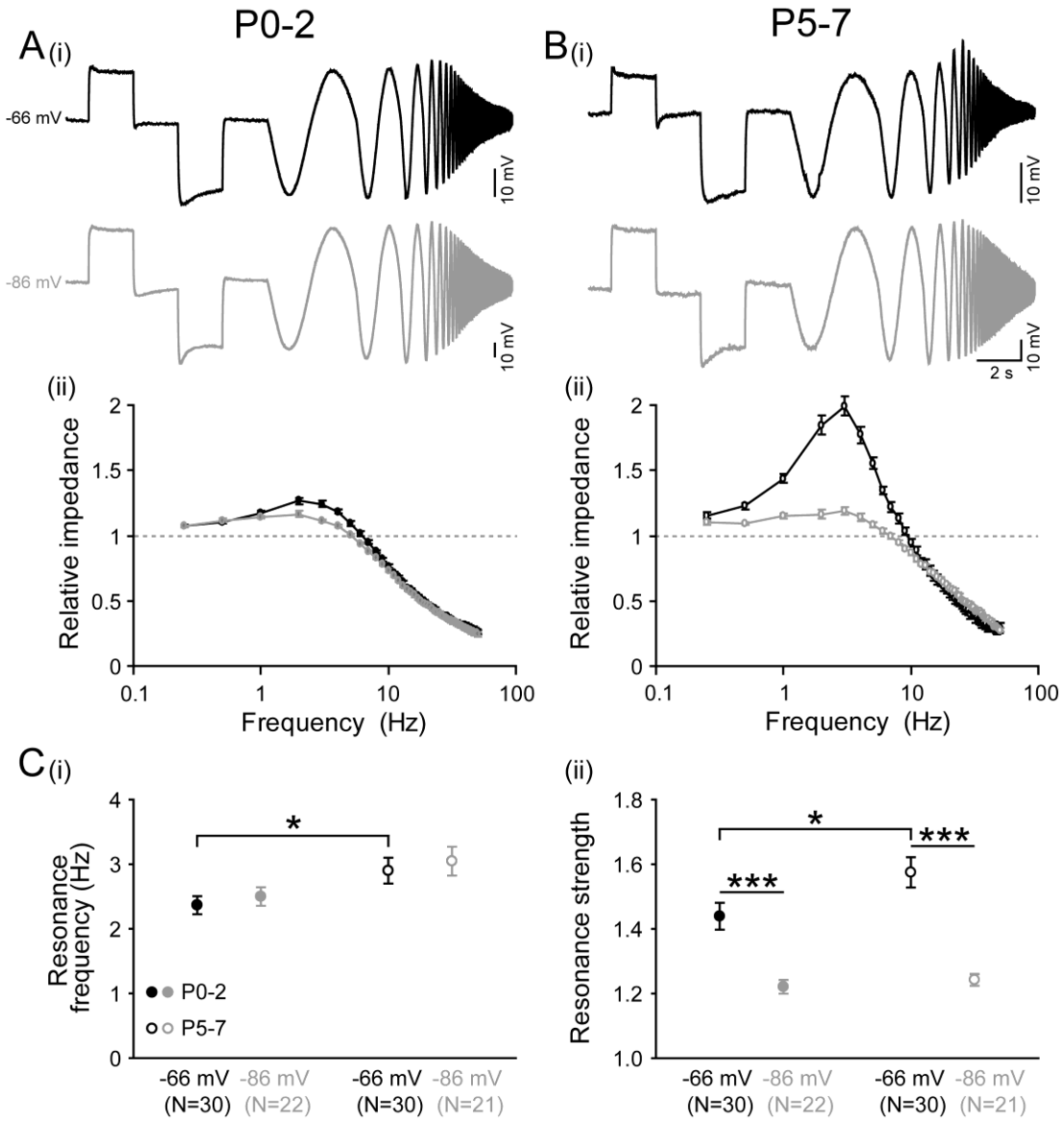

Fig. 7 Properties of subthreshold resonance in Cajal-Retzius cells.

A-B (i): Typical voltage responses of P0-P2 **(A)** and P5-P7 **(B)** Cajal-Retzius cells to sinusoidal current injection at a holding potential of -66 mV (black trace) and -86 mV (gray trace). Note that different current amplitudes were used to make the peak voltages comparable. **A-B (ii):** Frequency profile of the relative impedance from the recordings shown in **A(i)** and **B(i)**. Note that resonance strength decreased at a holding potential of -86 mV. **C:** Statistical analysis of resonance frequency **(i)** and strength **(ii)** recorded at different holding potentials and at different ages. Note that the resonance frequency and strength is significantly larger in P5-P7. The resonance frequency was unaffected by the holding potential, but resonance strength decreased significantly with hyperpolarization. All datapoints represent mean ± SEM. Statistical significant differences are marked by * ($P < 0.05$) and

*** ($P < 0.001$).

In order to investigate whether the pronounced hyperpolarization-activated cation current (I_h) in Cajal Retzius cells (Kilb and Luhmann, 2000) contribute to the resonance (Hutcheon et al., 1996), we used the highly selective I_h blocker ZD7288. In the presence of 10 µM ZD7288 the I_h was completely abolished (n=13, **Fig. 8A**) and the resonance was considerably attenuated (**Fig. 8B**). In total, the resonance strength was significantly (Sign-test, P = 0.0078 and p=0.0156, respectively) reduced to 1.07 ± 0.04 (n=8) in P0-P2 Cajal-Retzius cells and to 1.19 ± 0.07 (n=7) in P5-P7 Cajal-Retzius cells (**Fig. 8C**). In 5 out of 8 P0-P2 Cajal-Retzius cells and in 2 out of 7 P5-P7 Cajal-Retzius cells subthreshold resonance was completely abolished by ZD2788 (**Fig. 8D**). In addition, the cutoff frequency was significantly (U-tests, $U_{(36)}$ = 11, Z = -3.924, P < 0.001, and $U_{(35)}$ = 35.5, Z = -2.704, P = 0.0068, respectively) reduced to 3.6 ± 0.6 Hz (n=8) in P0-P2 and to 7.9 ± 1.4 (n=7) in P5-P7 Cajal-Retzius cells. In summary, these results suggest that in Cajal-Retzius cells I_h contributes considerably to the intrinsic resonance properties.

In order to investigate the obvious discrepancy between this strong role of I_h in subthreshold resonance, which should normally led to an increased resonance frequency upon hyperpolarization (Hutcheon et al., 1996), and the voltage independency of the resonance frequency in Cajal-Retzius cells, we analyzed the ZD-sensitive component of the impedance (**Fig. 8E**). This analysis revealed that at a holding potential of -86 mV the ZD-sensitive component of the impedance was negative, indicating that the already activated hyperpolarization-activated cation channels decreased the impedance throughout all frequencies. In contrast, at -66 mV the contribution of hyperpolarization-activated cation-channels to the impedance at low frequencies was significantly (Students t-test, $P < 0.05$ between 2 and 10 Hz) smaller, indicating that less hyperpolarization-activated cation channels are activated. Only at -66 mV activation of I_h channels between 2 and 8 Hz promoted an inductive component ($Z_{Ctrl} - Z_{ZD7288} > 0$) that enhanced the cell's impedance in this frequency

range (**Fig. 8E**).

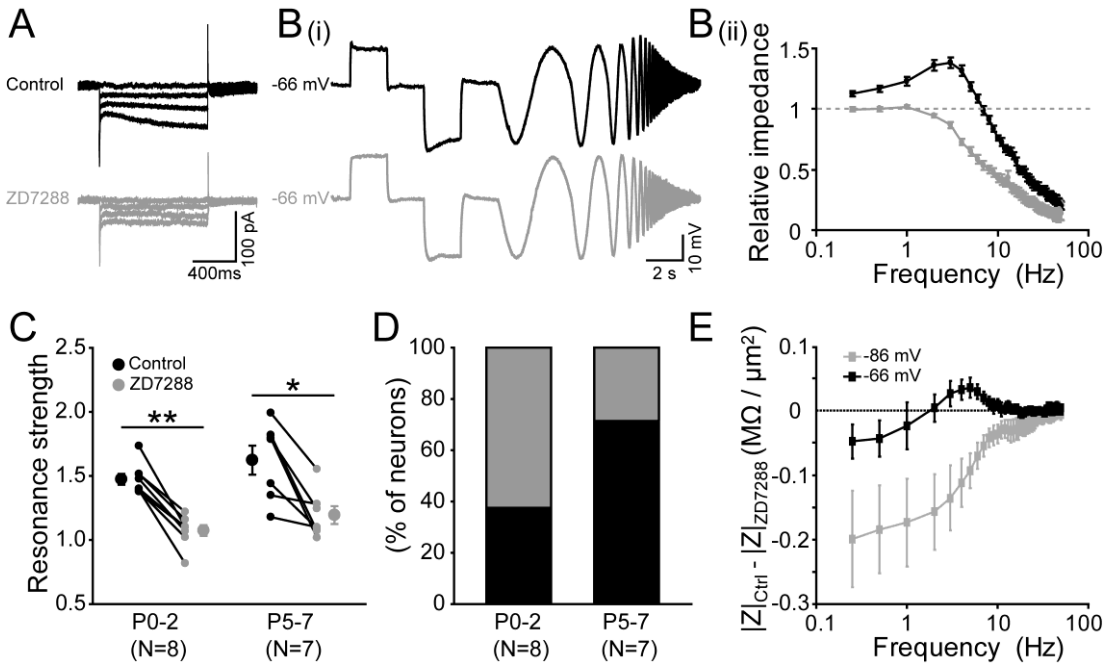

Fig. 8 Role of h current for subthreshold resonance of Cajal-Retzius cells.

A: Typical voltage-clamp recordings illustrating that administration of 10 µM ZD7288 (gray trace) abolished the slowly activating component of the inward current. **B:** Voltage response to sinusoidal current **(i)** and related frequency profile of the relative impedance **(ii)** before (black) and after (gray) application of ZD7288. Note the absence of resonance in the presence of ZD7288. **C:** Statistical analyses of the ZD effect on resonance strength in P0-2 (left) and P5-P7 (right) Cajal-Retzius cells. Note the massive decrease in resonance strength in the presence of ZD7288. **D:** Bar diagram illustrating the fraction of neurons showing complete blockade of resonance (gray) after applying ZD7288. In 5 out of 8 neurons in P0-P2 and 2 out of 7 neurons in P5-P7 resonance completely disappears. **E:** Frequency profile of the ZD7288-sensitive impedance component at holding potentials of -66 mV (black) and -86 mV (gray). Note the positive impedance values between 2 and 8 Hz at a holding potential of -66 mV. All datapoints represent mean ± SEM. Statistical significant differences are marked by * ($P < 0.05$) and ** ($P < 0.01$).

3.2 Properties and mechanisms of subthreshold resonance in supragranular pyramidal neurons

Whole-cell patch-clamp recordings were obtained from 15 P0-P2 CP and 60 P5-P7 layer II/III pyramidal neurons in mice coronal slices. Resting membrane potentials (-53.2 ± 3.1 mV and -62.2 ± 0.8 mV, respectively) and other membrane properties (**Table 1**) are in agreement with previous studies (Luhmann et al., 2000;Bahrey and Moody, 2003).

Analyses with sinusoidal current injection revealed that both CP neurons in the P0-P2 and layer II/III neurons in the P5-P7 neocortex showed subthreshold resonance at a holding potential of -66 mV. However, in both age groups a considerable portion of the neurons lacked subthreshold resonance (**Fig. 9A,B**). The fraction of resonant neurons was not significantly (Fisher's Exact Test, $P = 0.149$) different between P0-P2 CP neurons (53.3%; $n=15$) and P5-P7 layer II/III neurons (69.6%, $n=46$, **Fig. 9C**). The average resonance frequency of P0-P2 CP neurons was 1.5 ± 0.4 Hz ($n=8$), with a resonance strength of 1.20 ± 0.04 (**Fig. 9D**). Resonance frequency (1.3 ± 0.1 Hz, $n=32$) of P5-P7 layer II/III neurons was not significantly (U-test, $U_{(38)} = 124.5$, $Z = -0.127$, $P = 0.899$) different, but the resonance strength was significantly (U-test, $U_{(38)} = 65$, $Z = -2.13$, $P = 0.033$) higher (1.29 ± 0.02).

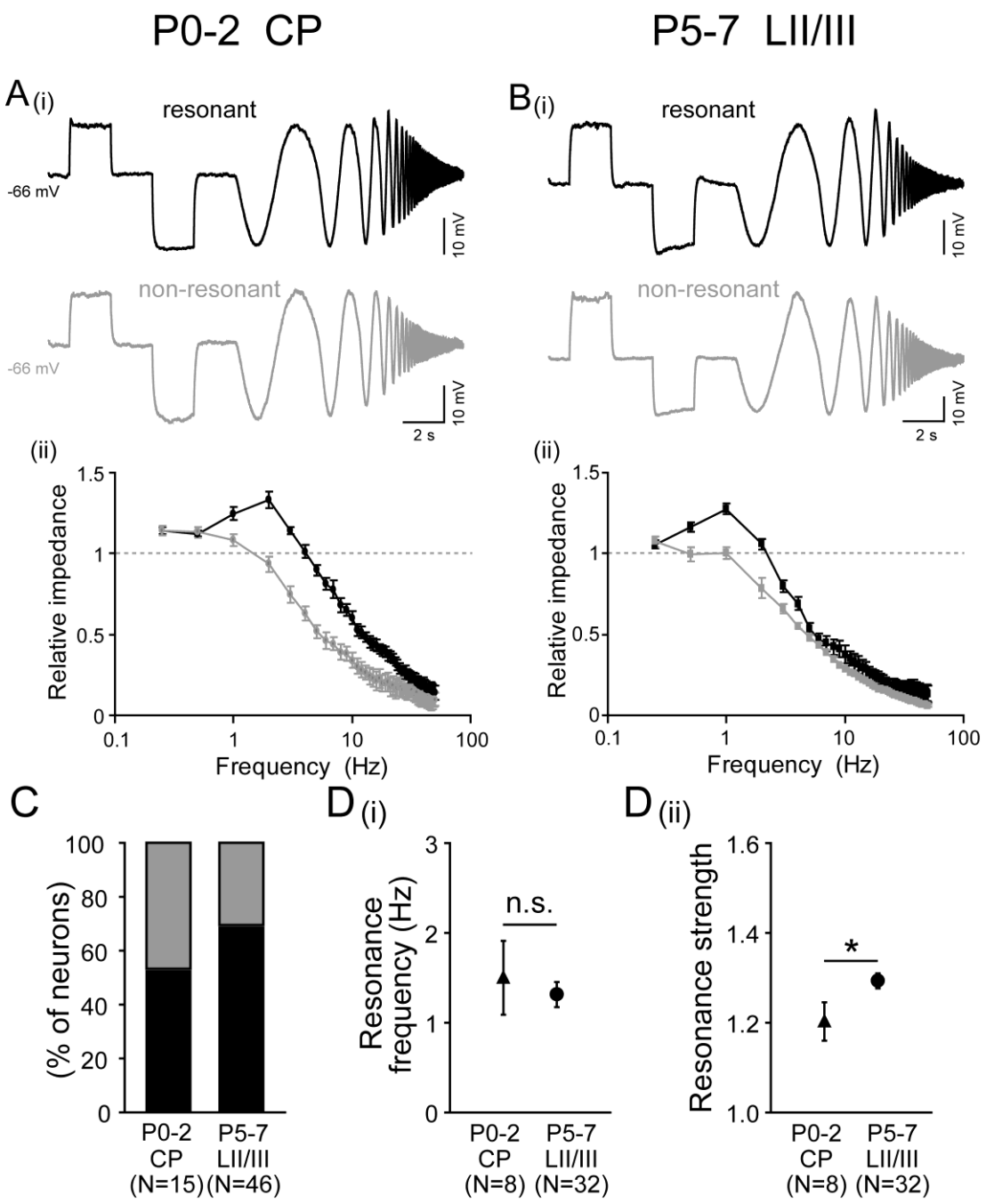

Fig. 9 Properties of subthreshold resonance in immature pyramidal neurons of supragranular neocortical layers.

A-B (i): Typical voltage response of resonant (black) and non-resonant (gray) pyramidal neuron at P0-P2 in the CP (left) and P5-P7 (right) in layer II/III to sinusoidal injection currents. **A-B (ii):** Frequency profile of the relative impedance from the recordings shown in **A(i)** and **B(i)**. Note that the relative impedance curve of non-resonant neurons declined monotonically. **C:** Bar diagram illustrating the fraction of resonant (black) and non-resonant (gray) neurons. **D:** Statistical analysis showing that

resonance frequency **(i)** was not significantly different between both age groups, but resonance strength **(ii)** was significantly higher in P5-P7 group. All datapoints represent mean ± SEM. Statistical significant differences are marked by * ($P < 0.05$).

To test whether resonance in layer II/III pyramidal neurons was voltage dependent, we measured subthreshold resonance in six P5-P7 layer II/III pyramidal neurons at -66 and -86 mV (**Fig. 10A**). However, neither resonance frequency (0.9 ± 0.2 Hz vs. 1 ± 0.2 Hz) nor resonance strength (1.21 ± 0.04 vs. 1.27 ± 0.07) was significantly (Sign-test, $P = 1$ and $P = 0.69$, respectively) different between -66 and -86 mV (**Fig. 10B**), suggesting that resonance is not voltage dependent.

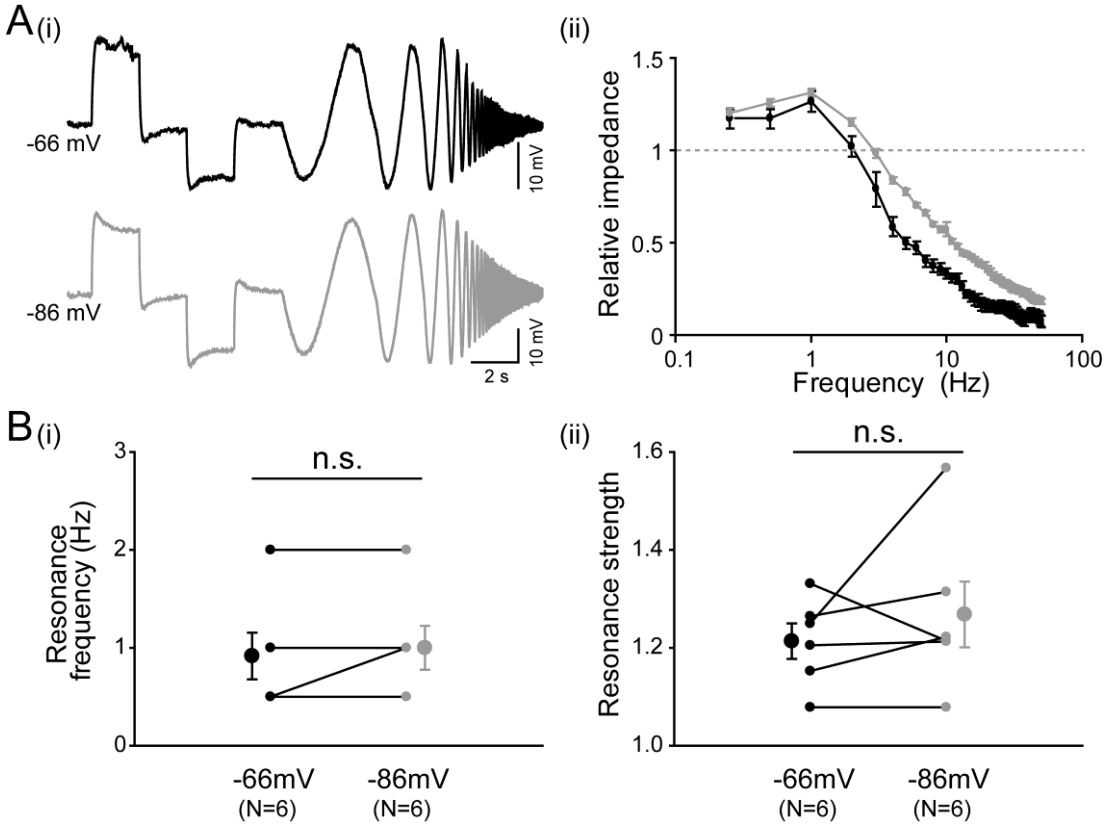

Fig. 10 Voltage independence of resonance behaviour in immature pyramidal neurons of supragranular neocortical layers.

A: Typical voltage responses of a pyramidal cell to sinusoidal current injection at a holding potential of -66 mV (black trace) and -86 mV (gray trace) **(i)** and corresponding frequency profile of the relative impedance **(ii)**. **B:** Statistical analyses revealed that resonance frequency **(i)** and strength **(ii)** are not significantly different between -66 mV and -86 mV. All datapoints represent mean ± SEM.

In layer II/III pyramidal neurons bath application of 10 µM ZD7288 at holding potential of -86 mV had no effect on subthreshold resonance (**Fig. 11A**). Neither resonance frequency (1.1 ± 0.1 Hz vs. 1.2 ± 0.2 Hz, *n*=10) nor strength (1.33 ± 0.07 vs. 1.44 ± 0.05, *n*=10) was significantly (Sign test, $P > 0.05$) affected by ZD7288 (**Fig. 11B**), suggesting that I_h does not considerably contribute to subthreshold resonance in layer II/III pyramidal neurons. In addition, the cutoff frequency was not significantly (Sign-test, $P = 1$) affected by ZD7288 (5.9 ± 0.4 Hz vs. 6.1 ± 0.8 Hz, *n*=10).

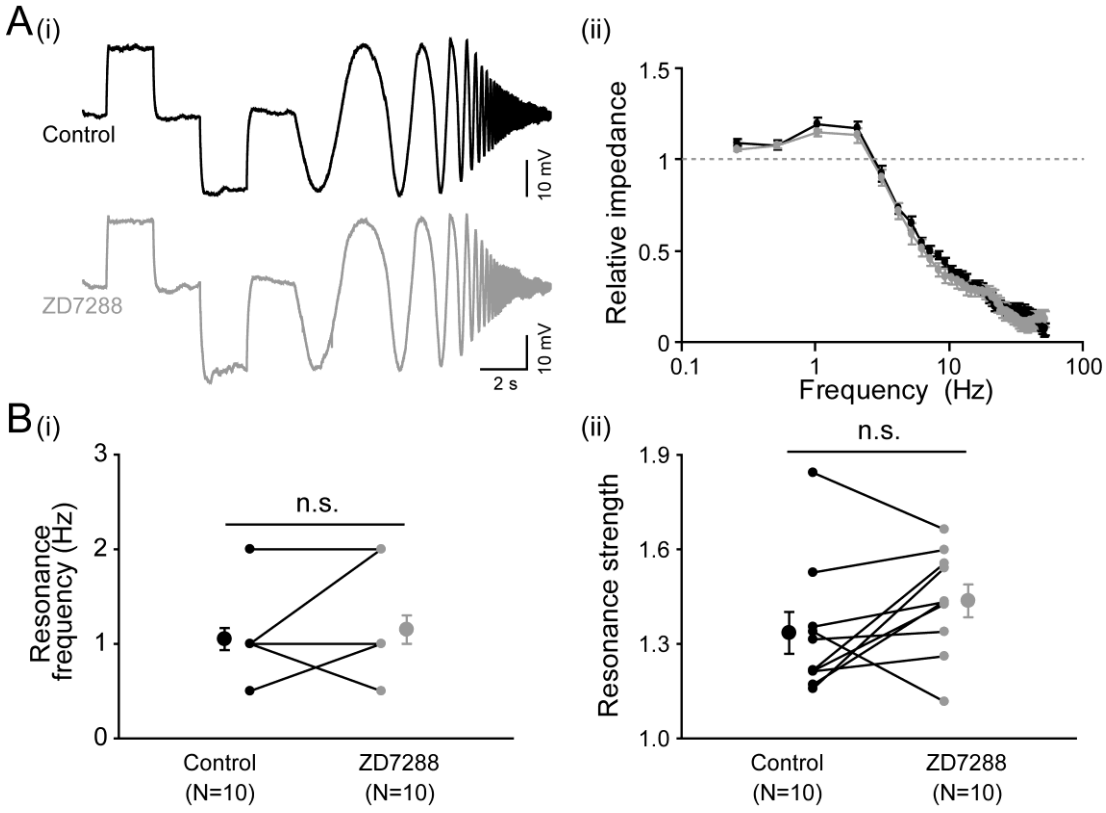

Fig. 11 H current is not involved in subthreshold resonance of immature pyramidal neurons of supragranular neocortical layers.

A: Typical voltage response to sinusoidal current injection **(i)** and related frequency profile of the relative impedance **(ii)** before (black) and after (gray) application of ZD7288. **B:** Statistical analyses of the ZD effect on resonance frequency and resonance strength in immature pyramidal neurons of supragranular neocortical layers. Note that the subthreshold resonance was unaffected by ZD7288. All datapoints represent mean ± SEM.

In contrast, bath application of 1 mM Ni^{2+}, a blocker of t-type Ca^{2+} currents (Puil et al., 1994;Perez-Reyes et al., 1998) attenuated subthreshold resonance (**Fig. 12A, B**). In the presence of Ni^{2+}, in 5 out of these 8 neurons no significant subthreshold resonance was observed in the presence of Ni^{2+} (**Fig. 12C**) and the resonance strength was significantly (Sign-test, P = 0.0078) reduced from 1.32 ± 0.06 to 1.17 ± 0.02 (n=8) (**Fig. 12D**). The cutoff frequency was not significantly (Sign-test, P = 0.375) affected in the presence of Ni^{2+} (4.4 ± 0.4 Hz vs. 3.9 ± 0.4 Hz, n=8). These results suggest that in layer II/III pyramidal neurons t-type Ca^{2+} channels contribute to the subthreshold resonance, while I_h does not play an essential role.

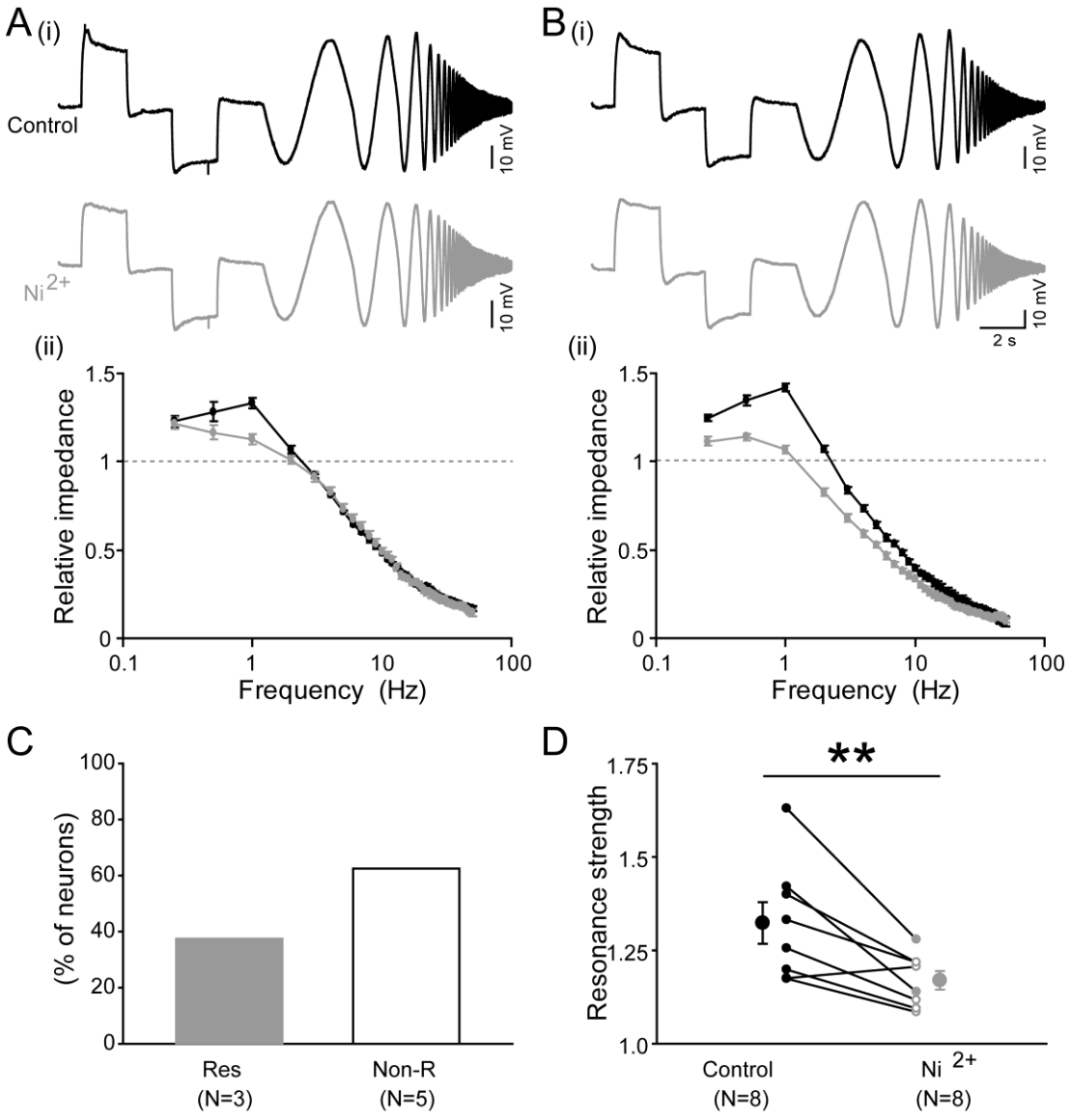

Fig. 12 Role of t-type Ca^{2+} currents for subthreshold resonance in immature pyramidal neurons of supragranular neocortical layers.

A-B: Typical voltage response to sinusoidal current injection **(i)** and corresponding frequency profile of the relative impedance **(ii)** before (black) and after (gray) application of Ni^{2+}. **C:** Bar diagram illustrating the fraction of resonant (gray) and non-resonant (white) neurons after application of Ni^{2+}. **D:** Statistical analysis of the resonance strength under control conditions (black) and after application of 1mM Ni^{2+} (gray). Open symbols represent recordings in which resonance was completely blocked. Note that the resonance was reduced in the presence of Ni^{2+}. All datapoints represent mean ± SEM. Statistical significant differences are marked by and ** ($P < 0.01$).

3.3 Properties and mechanisms of subthreshold resonance in layer V pyramidal

neurons

Whole-cell patch-clamp recordings were obtained from 16 P0-P2 and 87 P5-P7 layer V pyramidal neurons in mice coronal slices. Resting membrane potentials (-56.6 ± 1.4 mV and -64.6 ± 0.5 mV, respectively) and other membrane properties (**Table 1**) are in agreement with previous studies (Mccormick and Prince, 1987;Luhmann et al., 2000).

Layer V pyramidal neurons from both P0-P2 and P5-P7 cortices displayed similar resonance properties (**Fig. 13A, B**). Like supragranular pyramidal neurons, not all layer V pyramidal neurons showed resonance at a holding potential of -66 mV. No significant difference (Fisher's Exact Test, P = 0.103) in the fraction of resonant neurons was observed between both age groups, 50% of the P0-P2 (n=16) and 67.2% (n=61) of the P5-P7 pyramidal neurons showed subthreshold resonance (**Fig. 13C**). The average resonance frequency of P0-P2 layer V neurons was 1.1 ± 0.3 Hz (n=8), with a resonance strength of 1.30 ± 0.06 (**Fig. 13D**). Resonance frequency (1.5 ± 0.2 Hz, n=41) and strength (1.34 ± 0.02) of P5-P7 layer V neurons were not significantly different (U-tests, $U_{(47)}$ = 123.5, Z = -1.168, P = 0.243 and $U_{(47)}$ = 143, Z = -0.568, P = 0.570, respectively) (**Fig. 13D**).

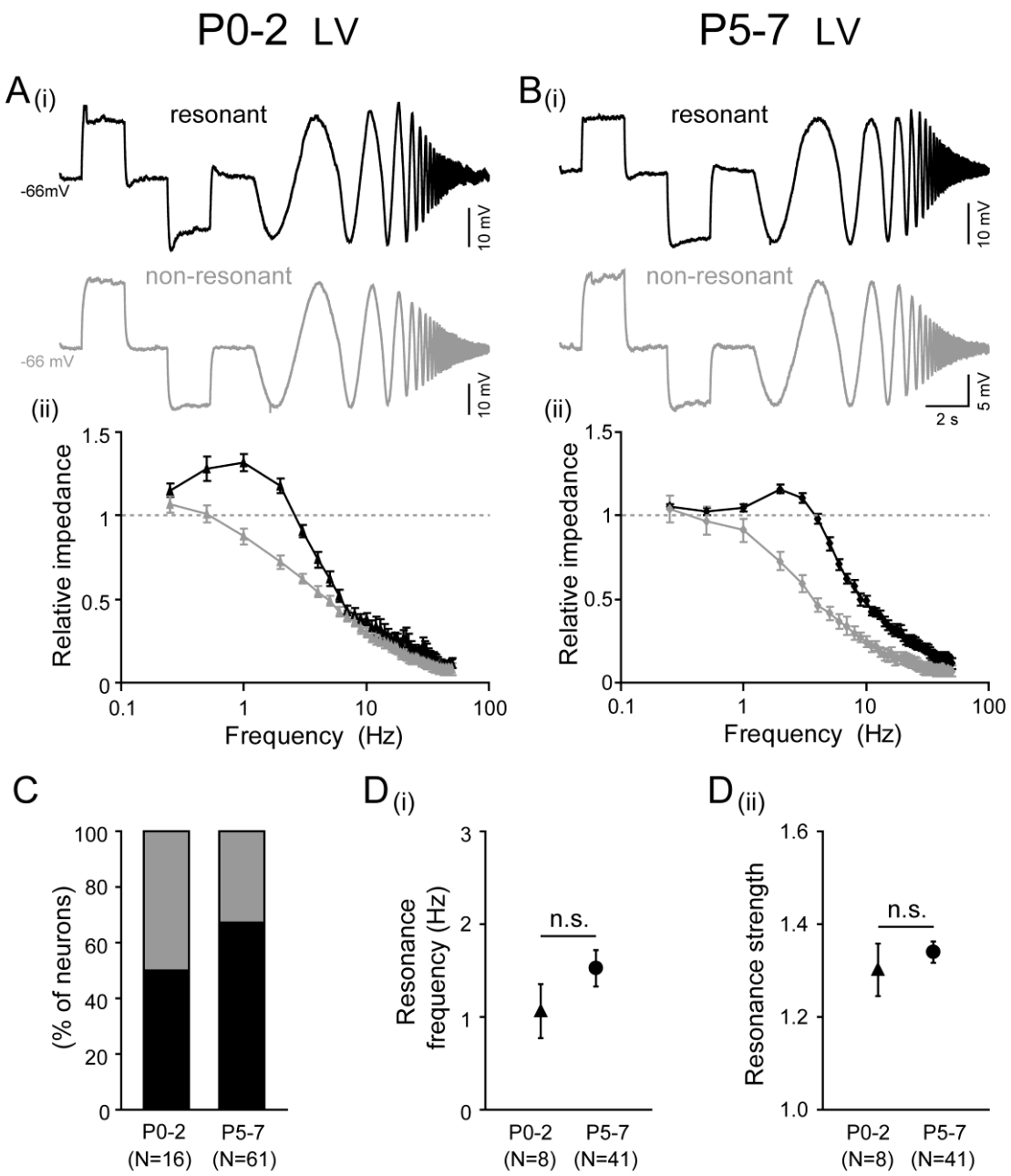

Fig. 13 Properties of subthreshold resonance in immature pyramidal neurons of layer V.

A-B (i): Typical voltage response of resonant (black) and non-resonant (gray) pyramidal neuron at P0-P2 (left) and P5-P7 (right) in layer V to sinusoidal injection currents. **A-B (ii):** Frequency profile of the relative impedance from the recordings shown in **A(i)** and **B(i)**. Note that the relative impedance curve of non-resonant neurons declined monotonically. **C:** Bar diagram illustrating the fraction of resonant (black) and non-resonant (gray) neurons. **D:** Statistical analysis showing that resonance frequency **(i)** and resonance strength **(ii)** were not significantly different between both age groups. All datapoints represent mean ± SEM.

To test whether resonance in layer V pyramidal neurons was voltage-dependent, we measured subthreshold resonance in 11 P5-P7 layer V pyramidal neurons at -66 mV and -86 mV (**Fig. 14A**). Hyperpolarizing the holding potential from -66 mV to -86 mV significantly (Sign test, $P = 0.0156$) shifted resonance frequency from 1.0 ± 0.16 (n=11) to 2 ± 0.23 Hz, while the resonance strength was not significantly affected (**Fig. 14B**). Moreover, at holding membrane potential of -66 mV, 67.7% (n=62) of the P5-P7 layer V pyramidal neurons showed subthreshold resonance. However, when holding at -86 mV, all neurons (n=24) exhibited subthreshold resonance (**Fig. 14C**), all these results suggesting that resonance in layer V pyramidal neurons is voltage-dependent.

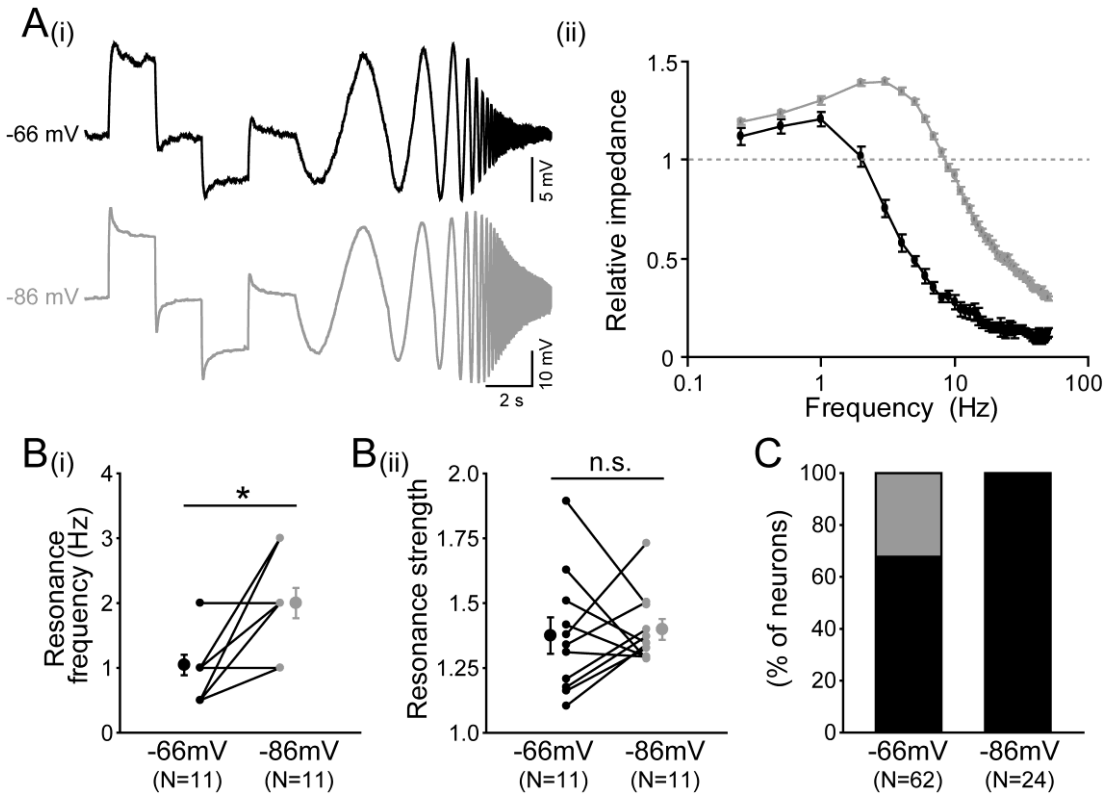

Fig. 14 Voltage dependence of resonance behaviour in immature pyramidal neurons of layer V.

A: Typical voltage responses of a layer V pyramidal cell to sinusoidal current injection at a holding potential of -66 mV (black trace) and -86 mV (gray trace) **(i)** and corresponding frequency profile of the relative impedance **(ii)** from the traces shown in **A(i). B:** Statistical analysis showing that resonance frequency **(i)** was significantly higher when holding at -86 mV, but resonance strength **(ii)**

was not significantly different between -66 mV and -86 mV. **C:** Bar diagram illustrating the fraction of resonant (black) and non-resonant (gray) neurons. All datapoints represent mean ± SEM. Statistical significant differences are marked by * ($P < 0.05$).

Bath application of 10 µM ZD7288 abolished the I_h in all layer V pyramidal neurons tested (n=9, **Fig. 15A**). Subthreshold resonance was completely suppressed in the presence of 10 µM ZD7288 in all 17 investigated layer V pyramidal neurons (**Fig. 15B**). Accordingly the cutoff frequency was significantly (Sign-test, $P < 0.001$) shifted from 10.4 ± 0.8 to 2.2 ± 0.3 Hz (n=17). Because the effects of ZD7288 could not be reversed after washout (Hu et al., 2002) we performed additional experiments with Cs^+ to reversible block I_h (**Fig. 15C**). In the presence of 1 mM CsCl I_h was reversibly reduced by 22±2.9% (n=10, **Fig. 15C**). In accordance with this partial I_h antagonism, CsCl reduced subthreshold resonance (**Fig. 15D**). The resonance strength was significantly (Sign test, $P = 0.005$) attenuated from 1.49 ± 0.04 to 1.31 ± 0.03 (n=12) and the resonance frequency significantly (U-test, $U_{(19)} = 7.5$, $Z = -3.561$, $P < 0.001$) decreased from 1.8 ± 0.1(n=12) to 0.8 ± 0.09 (n=9). In 3 out of these 12 layer V pyramidal neurons no significant subthreshold resonance could be observed in the presence of 1 mM CsCl. The resonance frequency recovered to control level of 1.6 ± 0.2 (n=7) after washout (**Fig. 15E**). In addition, the cutoff frequency was significantly (Sign test, $P < 0.001$) reduced from 10.3 ± 0.6 to 4 ± 0.3 Hz (n=12). In summary, these results suggest that in layer V pyramidal neurons I_h considerably contributes to the resonance properties.

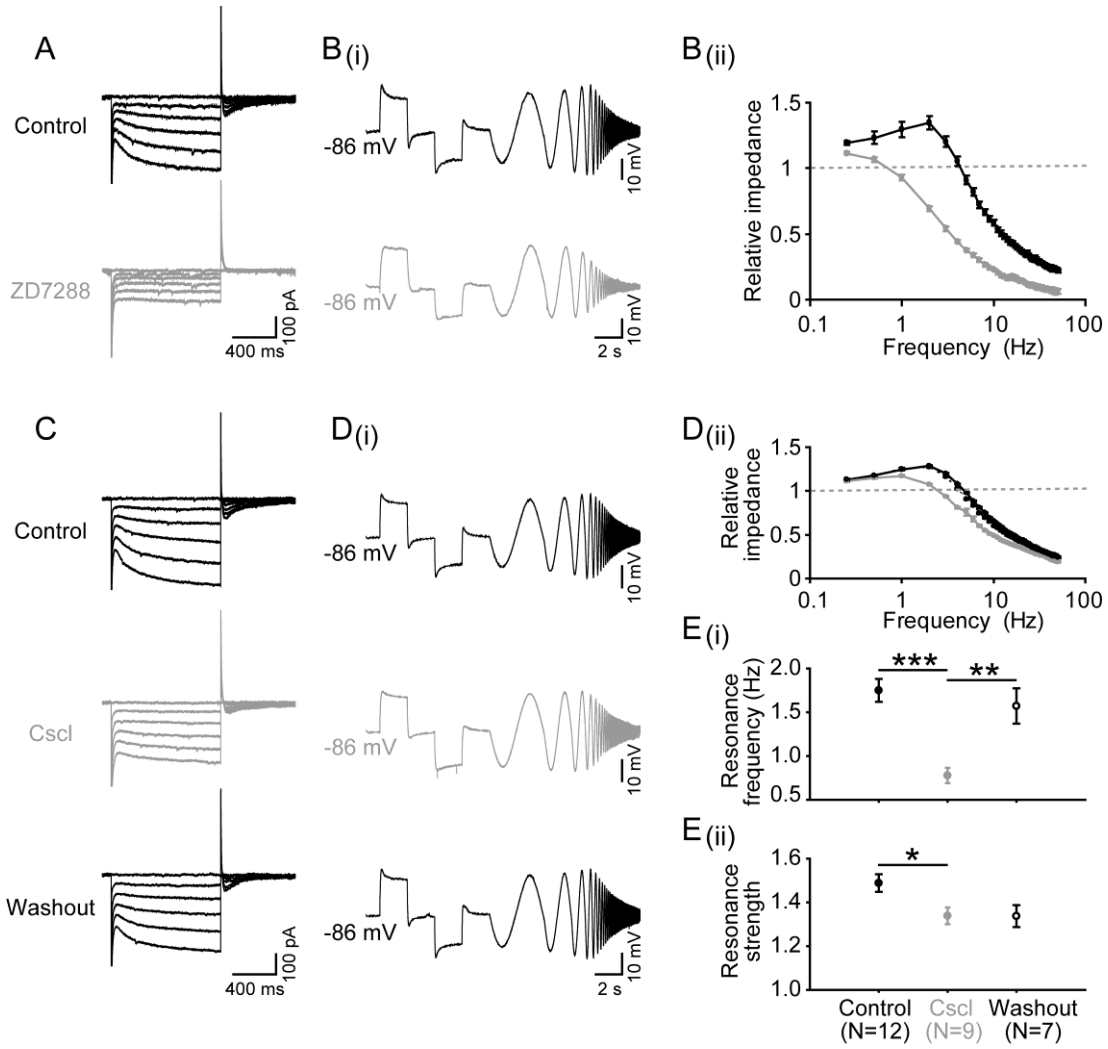

Fig. 15 Role of h current for subthreshold resonance in immature pyramidal neurons of layer V.

A: Typical voltage-clamp recordings illustrating that administration of 10 μM ZD7288 (gray trace) abolished the slowly activating component of the inward current. **B:** Voltage response to sinusoidal current **(i)** and related frequency profile of the relative impedance **(ii)** before (black) and after (gray) application of ZD7288. Note the absence of resonance in the presence of ZD7288. **C:** Typical voltage-clamp recordings illustrating that administration of 1 mM Cs^+ attenuated the slowly activating component of the inward current, which could be reversed after washout of 1 mM Cs^+. **D:** Voltage response to sinusoidal current injection **(i)** and corresponding frequency profile of the relative impedance **(ii)** before (black), after (gray) application and after washout of 1mM CsCl. Note the decrease in resonance frequency and resonance strength in the presence of CsCl, which could be reversed after washout of CsCl. **E:** Statistical analyses of resonance frequency **(i)** and resonance strength **(ii)** in 9 out of 12 cells in which resonance persisted in the presence of CsCl. Note the

significant decrease in resonance frequency in the presence of CsCl, which could be reversed after washout. All datapoints represent mean ± SEM. Statistical significant differences are marked by * ($P < 0.05$) ** ($P < 0.01$) and *** ($P < 0.001$).

3.4 Properties of subthreshold resonance in subplate neurons

Whole-cell patch-clamp recordings were obtained from 45 P0-P2 and 14 P5-P7 subplate neurons in mice coronal slices. Resting membrane potentials (-53.8 ± 0.8 mV and –57 ± 1.8 mV, respectively) and other membrane properties (**Table 1**) are in agreement with previous studies (Luhmann et al., 2000;Hanganu et al., 2002).

Both resonant and non-resonant subplate neurons were observed (**Fig. 16A-B**). No significant differences (Fisher's Exact Test, $P = 0.24$) in the percentage of resonant neurons could be observed between P0-P2 (44.4%) and P5-P7 (42.9%) subplate neurons (**Fig. 16C**). Subplate neurons from P0-P2 cortices had a resonance frequency of 1.4 ± 0.2 Hz (n=20) and a resonance strength of 1.30 ± 0.03. The resonance properties of P5-P7 were not significantly (U-tests, $U_{(24)} = 75$, $P = 0.338$ and $U_{(24)} = 87$, $P = 0.10$, respectively) different, they showed a resonance frequency of 0.8 ± 0.1 Hz (n=6) and a resonance strength of 1.20 ± 0.03 (**Fig. 16D**)." (from Sun etal., 2012).

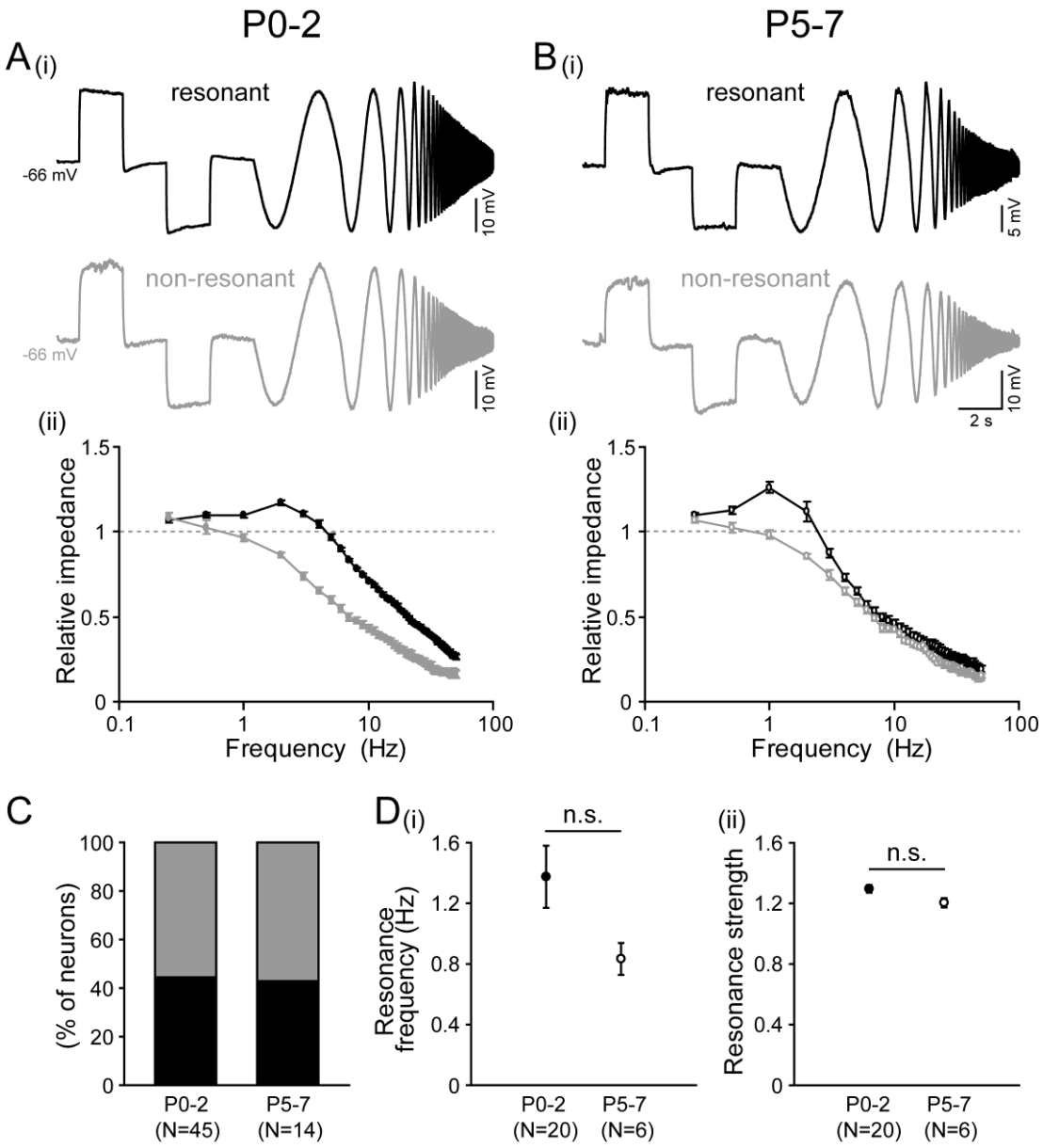

Fig. 16 Properties of subthreshold resonance in subplate neurons.

A-B: Typical voltage responses of resonant (black) and non-resonant (gray) subplate neurons **(i)** of P0-P2 **(A)** and P5-P7 **(B)** and corresponding frequency profile of the relative impedance at a holding potential of -66 mV **(ii). C:** Bar diagram illustrating the fraction of resonant (black) and non-resonant (gray) subplate neurons. **D:** Statistical analysis showing that resonance frequency **(i)** and strength **(ii)** have no significant difference between different age groups. All datapoints represent mean ± SEM.

3.5 Electrical properties of immature cortical GABAergic interneurons

Whole-cell patch-clamp recordings were obtained from 56 P6-P9 and 41 P10-P13 GABAergic interneurons from GAD67-GFP transgenic mice. Interneurons from P6-9 and P10-13 animals showed a comparable resting membrane potential of –64.4 ± 1.0 mV (n=56) and –67.9 ± 1.2 mV (n=41), respectively. P6-9 interneurons had a R_{in} of 0.96 ± 0.08 GΩ and a C_{in} of 71.3 ± 5.1 pF (n=56). In P10-13 interneurons R_{in} (0.48 ± 0.05 GΩ) was significantly ($P<0.001$) smaller and C_{in} (101.9 ± 7.8 pF) was significantly ($P<0.01$) larger (n=41) (**Table 1**).

All recorded GAD67-GFP interneurons displayed repetitive action potentials (AP) with a relatively high discharge frequency and little spike adaptation (**Fig. 17B i**). The active membrane properties showed a considerable refinement between P6 and P13. While the AP amplitude was comparable ($P=0.790$) between P6-9 (63.4 ±1.4 mV, n=56) and P10-13 interneurons (66.3 ± 1.2 mV, n=41), AP threshold was not significantly ($p=0.089$) higher in interneurons from P10-13 animals than in those from P6-9 animals (P6-9: –42.4 ± 0.4 mV vs. P10-13: –40.6 ± 0.5 mV). Interneurons from P10-13 animals showed a significantly shorter AP duration (2.1 ± 0.1 vs. 1.5 ± 0.1, $P<0.05$) due to a significantly faster rise (101 ± 5.4 V/s vs. 137 ± 5.4 V/s) and decay (–37 ± 2.7 V/s vs. –46 ± 2.1 V/s) of the spike (**Fig. 17Bii**). In accordance with this shorter AP duration, maximal spike frequency was significantly ($P<0.05$) higher in P10-13 interneurons (52 ± 1.9 Hz vs. 69 ± 3 Hz, **Fig. 17Biii**).

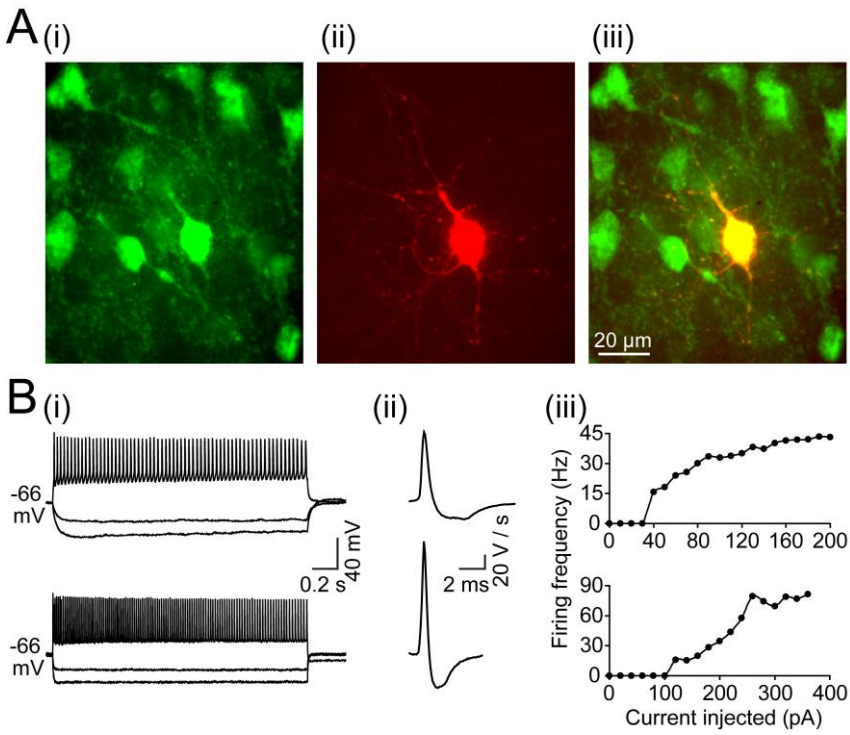

Fig. 17 Identification of GABAergic interneurons in the immature cerebral cortex.

A: Photomicrograph of immunohistochemically stained GFP^+ GABAergic interneurons in a coronal slice **(i)**, the biocytin-labeled recorded neuron **(ii)** and the merged picture **(iii). B:** Characteristic response pattern of interneuron from a P8 (upper traces) and a P10 (lower traces) GAD67-GFP mouse upon injection of de- and hyperpolarizing currents **(i)**. Action potentials of the P10 interneuron (lower panels) displayed higher de- and repolarization rates **(ii)** and a higher maximal frequency **(iii)** as compared to the P8 interneuron (upper panels).

3.6 Properties of subthreshold resonance in GABAergic interneurons

We used the injection of sinusoidal current to identify GAD67-GFP interneurons that show subthreshold resonance. In about 50% of all investigated interneurons a significant subthreshold resonance was observed, while the remaining neurons showed passive low-pass filtering properties (**Fig. 18A**). No significant differences in the fraction of resonant interneurons could be observed between P6-P9 (53.2%) and P10-P13 (51.5%) neocortical slices (**Fig. 18B**). Interneurons from P6-P9 cortices had a resonance frequency of 2.3 ± 0.3 Hz (n = 25) and resonance strength of 1.16 ± 0.02 when recorded from a holding potential of –66 mV. Resonance

properties of P10-P13 interneurons were not significantly (P>0.05) different: they showed a resonance frequency of 1.6 ± 0.2 Hz (*n* =17) and resonance strength of 1.15 ± 0.02 (**Fig. 18C**). At a more hyperpolarized holding potential of –86 mV subthreshold resonance was considerably attenuated. For P6-P9 interneurons the resonance frequency significantly dropped to 1.3 ± 0.17 Hz (n=12; P=0.02) and the resonance strength to 1.11 ± 0.02 (P=0.0238). For P10-P13 interneurons the resonance frequency was non-significantly reduced to 1.1 ± 0.18 Hz (n=14, P=0.058), while a significant (P=0.002) reduction in the resonance strength to 1.1 ± 0.01 (n=14) was observed. Neither the incidence of resonance nor the preferred resonance frequency showed a correlation with the maximal firing frequency of the neurons (data not shown), indicating that the resonance properties were uniform among the whole interneuron population. In summary, these experiments show that a substantial fraction of developing interneurons display a weak subthreshold resonance in the delta frequency range.

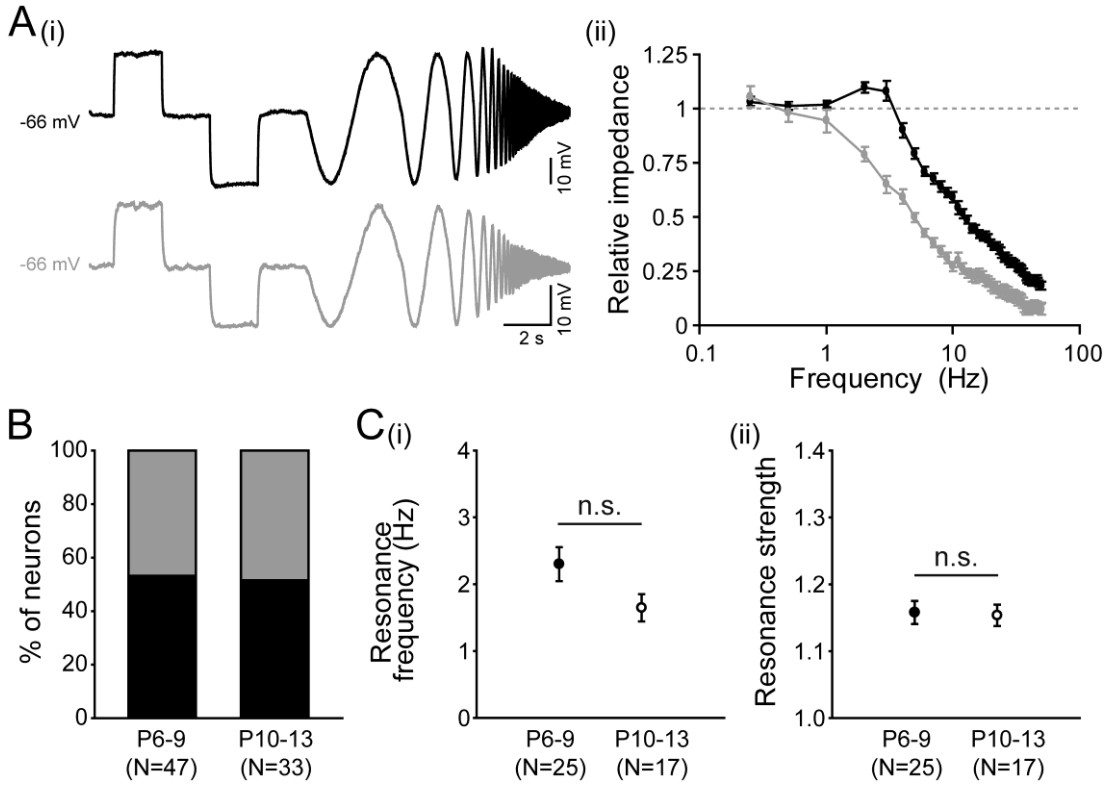

Fig. 18 Properties of subthreshold resonance in GABAergic interneurons.

A: Typical voltage responses of resonant (black trace) and non-resonant (gray trace) interneurons **(i)**

and corresponding frequency profile of the relative impedance at a holding potential of –66 mV **(ii). B:** Bar diagram illustrating the fraction of resonant (black) and non-resonant (gray) interneurons in the different age groups. **C:** Statistical analysis illustrating that resonance frequency **(i)** and strength **(ii)** show no significant difference between different age groups. Datapoints represent mean ± SEM.

3.7 Role of t-type Ca^{2+} currents for resonance of GABAergic interneurons

In order to unravel whether t-type Ca^{2+} currents underlie the resonance of GABAergic interneurons (Puil et al., 1994;Hutcheon and Yarom, 2000), we next analyzed whether subthreshold resonance was affected by Ni^{2+}, a relatively selective blocker of t-type Ca^{2+} currents (Ertel and Ertel, 1997;Perez-Reyes et al., 1998). These experiments revealed that bath application of 1 mM Ni^{2+} attenuated subthreshold resonance at holding potential of –66 mV (**Fig. 19A**). In the presence of Ni^{2+} the resonance strength was significantly (P=0.0156) reduced from 1.11 ± 0.01 to 1.06 ± 0.02 (n=7). In 5 out of these 7 neurons no significant subthreshold resonance was observed in the presence of Ni^{2+} (**Fig. 19A**). At a holding potential of –86 mV bath application of 1 mM Ni^{2+} has a comparable effect on subthreshold resonance (**Fig. 19B**). At this hyperpolarized holding potential the resonance strength was reduced from 1.08 ± 0.01 to 1.05 ± 0.01 (n=8) in the presence of Ni^{2+}. In 6 out of these 8 neurons no significant subthreshold resonance was observed in the presence of Ni^{2+} (**Fig. 19B**). In summary, these results demonstrate that t-type Ca^{2+} channels are essential for the generation of subthreshold resonance in immature GABAergic interneurons.

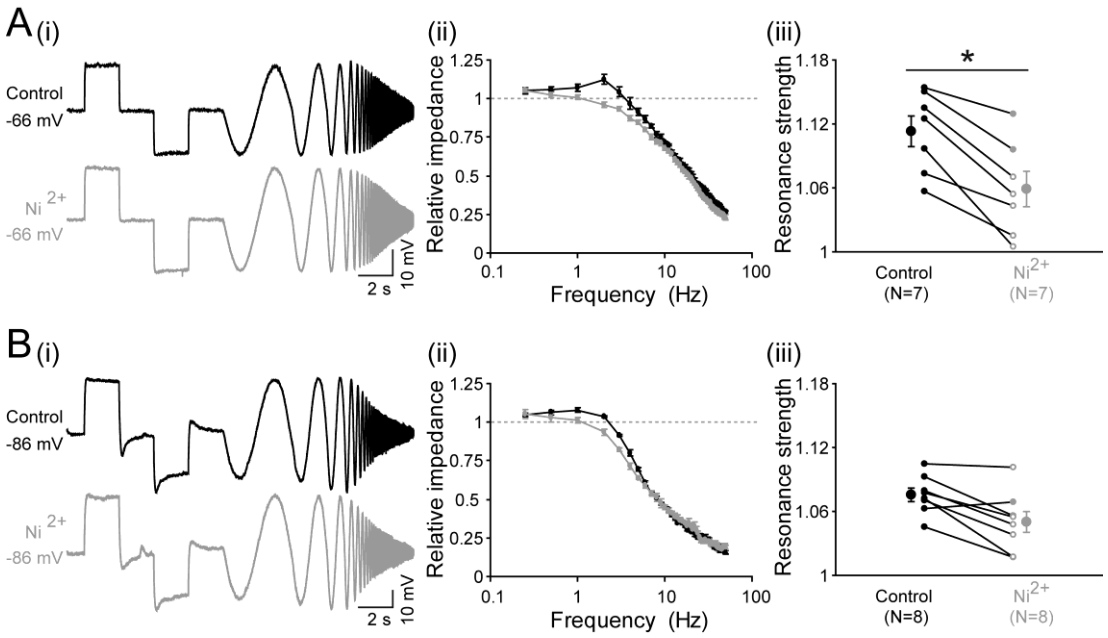

Fig. 19 Role of t-type Ca^{2+} currents for subthreshold resonance of GABAergic interneurons.

A: Typical voltage response at –66 mV to sinusoidal current injection **(i)**, corresponding frequency profile **(ii)**, and statistical analysis of the resonance strength **(iii)** under control conditions (black) and after application of 1 mM Ni^{2+} (gray). Open symbols represent recordings in which no significant resonance was observed. B: Typical voltage response at –86 mV to sinusoidal current injection **(i)**, corresponding frequency profile **(ii)** and statistical analysis of the resonance strength **(iii)** under control conditions (black) and after application of 1mM Ni^{2+} (gray). Note that the resonance was attenuated in the presence of Ni^{2+}. Datapoints represent mean ± SEM. Statistical significant differences are marked by *($p<0.05$).

3.8 Role of hyperpolarization-activated cation currents for subthreshold resonance

Hyperpolarization-activated cation currents (I_h) have been shown to underlie subthreshold resonance (Hutcheon et al., 1996;Pape, 1996). To investigate whether I_h contribute to the resonance in GABAergic interneurons, we used the highly selective I_h blocker ZD7288 (Maccaferri and Mcbain, 1996). Bath application of 10 µM ZD7288 significantly (P=0.0313) reduced I_h in GABAergic interneurons by 61.4 ± 12.5 % (*n*=6, **Fig. 20A**). However, further experiments showed that the subthreshold resonance (recorded at holding potential of –66 mV) was not affected in the presence

of 10 µM ZD7288 (**Fig. 20B**). Neither resonance frequency (1.2 ± 0.2 Hz vs. 1.0 ± 0.2 Hz, n=7) nor strength (1.12 ± 0.01 vs. 1.12 ± 0.02, n=7) was significantly (P>0.05) altered **(Fig. 20C**), suggesting that I_h does not considerably contribute to subthreshold resonance in GABAergic interneurons.

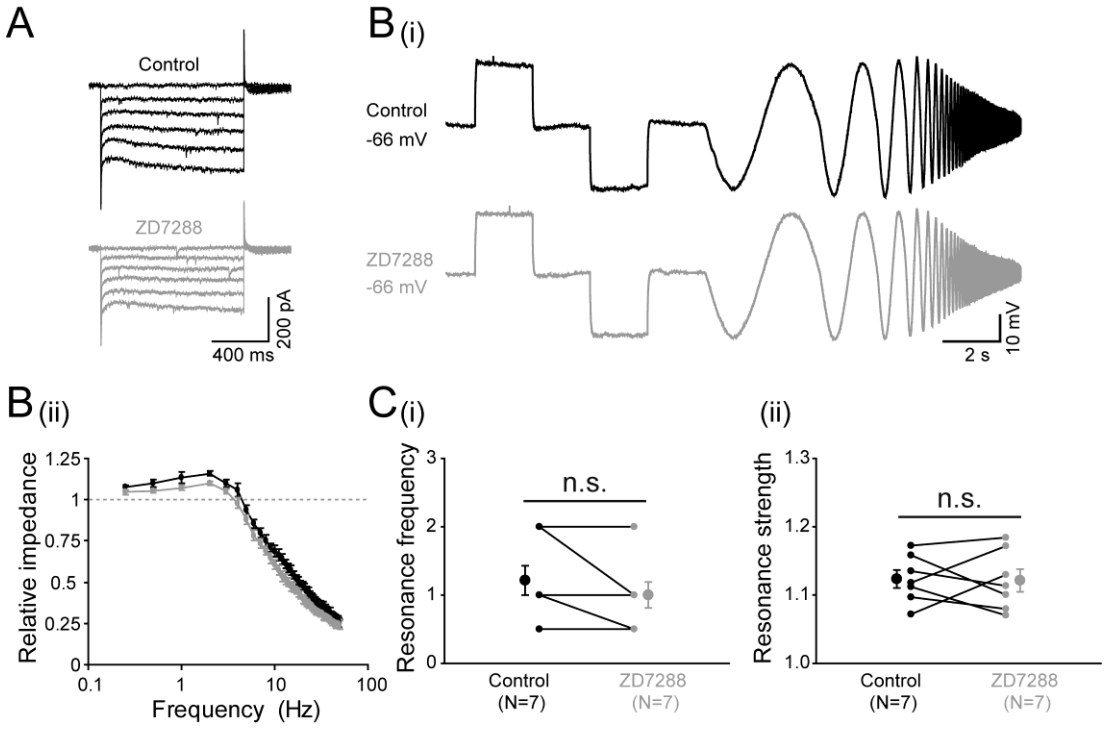

Fig. 20 The hyperpolarization-activated current (I_h) is not involved in subthreshold resonance of GABAergic interneurons.

A: Typical voltage-clamp recordings illustrating that administration of 10 µM ZD7288 (gray trace) reduced the slowly activating component of the inward current. **B:** Voltage response to sinusoidal current **(i)** and corresponding frequency profile of the relative impedance **(ii)** before (black) and after (gray) application of ZD7288. Note that subthreshold resonance was unaffected by ZD7288. **C:** Statistical analysis showing that resonance frequency **(i)** and strength **(ii)** were unaffected by ZD7288. Datapoints represent mean ± SEM.

3.9 Role of persistent sodium currents for subthreshold resonance

A variety of studies demonstrated that persistent Na^+ currents (I_{NaP}) are critically involved in the generation of subthreshold oscillations, in particular by amplifying

voltage responses generated by other currents (Hutcheon and Yarom, 2000). In order to investigate whether I_{NaP} contribute to the resonance in GABAergic interneurons, we first showed that I_{NaP} can be isolated in these neurons, using a slow voltage ramp protocol (**Fig. 21A**). A slow depolarization from –96 to –36 mV in 2 s caused the inactivation of the fast transient Na^+ current underlying the action potentials, preserving only the non-inactivating I_{NaP} (Wang et al., 2006). In accordance with previous reports (Puil et al., 1994;Hu et al., 2002;Wang et al., 2006), this I_{NaP} was absent in the presence of 400 nM TTX (**Fig. 21Ai**). The TTX-sensitive component of the current, resembling I_{NaP}, activated at a threshold of –52 ± 2.4 mV (n=7) and had an amplitude of 15 ± 5 pA (n=7) at –40 mV (**Fig. 21Aii**).

Bath application of 400 nM TTX also massively attenuated subthreshold resonance at holding potential of –66 mV (**Fig. 21B**). In the presence of TTX the resonance strength was significantly (P=0.0002) reduced from 1.18 ± 0.02 to 1.04 ± 0.01 (n=13). In 11 out of these 13 neurons no significant subthreshold resonance was observed in the presence of TTX (**Fig. 21B**). In contrast, bath application of 400 nM TTX at holding potential of –86 mV had no obvious effect on subthreshold resonance (**Fig. 21C**). Neither resonance frequency (1.2 ± 0.2 Hz vs. 1.3 ± 0.2 Hz, n=10) nor strength (1.13 ± 0.03 vs. 1.10 ± 0.01, n=10) was significantly affected by TTX (**Fig. 21C**). These results show that I_{NaP} contribute to the subthreshold resonance of GABAergic interneurons only at depolarized, but not at hyperpolarized potentials.

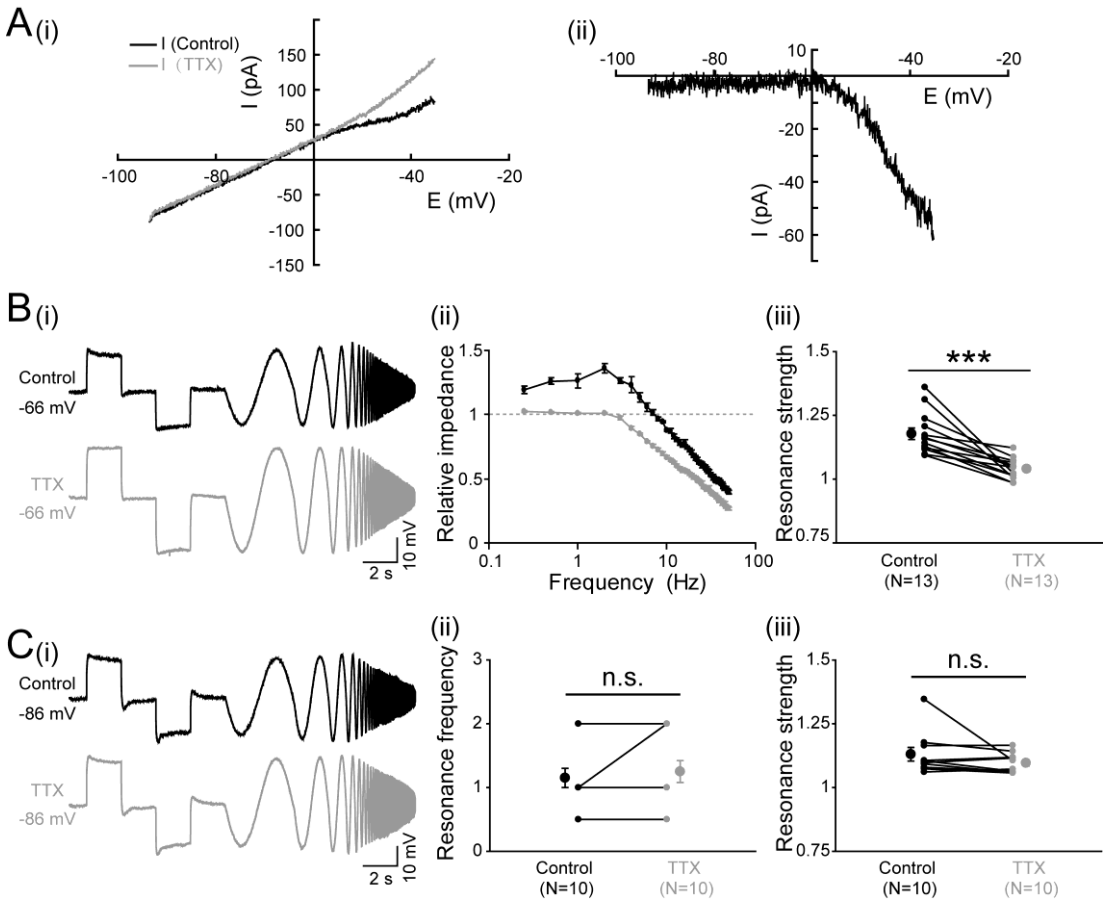

Fig. 21 Role of persistent Na^+ currents for the subthreshold resonance of GABAergic interneurons.

A: (i) Typical example of currents in response to a voltage ramp from –96 to –36 mV before (black trace) and after (gray trace) application of TTX (400 nM). **(ii)** TTX-sensitive current component obtained by subtracting the current in response to the ramp command before and after application of TTX. **B:** Typical voltage response at –66 mV to sinusoidal current injection **(i),** corresponding impedance spectrogram **(ii)**, and statistical analysis **(iii)** of the resonance strength under control condition (black) and after application of TTX (gray). Note that resonance was abolished in the presence of 400 nM TTX. **C:** Typical voltage response at –86 mV to sinusoidal current injection **(i),** corresponding impedance spectrogram **(ii)**, and statistical analysis **(iii)** of the resonance strength under control condition (black) and after application of TTX (gray). Note that subthreshold resonance frequency and strength was unaffected by TTX. Datapoints represent mean ± SEM. Statistical significant differences are marked by *** ($p<0.001$).

4. Discussion

In this study we investigated the properties of subthreshold resonance in Cajal-Retzius cells, supragranular pyramidal neurons, layer V pyramidal neurons, and subplate cells in the immature cerebral neocortex of C57BL/6 mice as well as GABAergic interneurons in the immature neocortex of GAD67-GFP transgenic mice. The findings of the present study can be summarized as follow: (i) Subthreshold resonance could be observed in all investigated neuronal cell types in the immature neocortex. (ii) While all Cajal-Retzius cells displayed subthreshold resonance, in supragranular pyramidal neurons, layer V pyramidal neurons, subplate cells and GABAergic interneurons both resonant and non-resonant neurons were observed. (iii) In all neuronal cell types the average resonance frequency was rather low in the delta frequency range. (iv) In Cajal-Retzius cells and layer V pyramidal cells the resonance was mainly caused by a hyperpolarization-activated cation current (I_h), in supragranular pyramidal neurons it was caused by t-type Ca^{2+} channels and in GABAergic interneurons the resonance was mainly caused by t-type Ca^{2+} channels and requires persistent sodium currents at depolarized membrane potentials. In summary, these results suggest that already in the early developing neocortex many neurons are capable to subthreshold resonance, however, at a rather low frequency.

4.1 Age-dependent electrophysiological properties of a variety of neuronal populations in the immature mouse neocortex

We observed a substantial developmental shift in the active and passive membrane properties of Cajal-Retzius cells, supragranular pyramidal neurons, layer V pyramidal neurons, subplate neurons and GABAergic interneurons, in accordance with previous studies (Kim et al., 1995;Zhou and Hablitz, 1996;Hestrin and Armstrong, 1996;Radnikow et al., 2002;Zhang, 2004;Christophe et al., 2005;Doischer et al., 2008;Okaty et al., 2009).

First in Cajal-Retzius cells, we found they displayed typical electrophysiological characteristics during the first postnatal week. They showed a relatively depolarized average resting membrane potential (RMP), had a high input resistance, expressed small amplitude and long half-width action potential (Kim et al., 1995;Zhou and Hablitz, 1996;Hestrin and Armstrong, 1996;Kilb and Luhmann, 2000;Radnikow et al., 2002). In addition, their AP amplitude increased and duration decreased with postnatal development. However, no obvious change in resting membrane potential with age was observed during the first postnatal week, as described by (Zhou and Hablitz, 1996;Radnikow et al., 2002). For supragranular pyramidal neurons and layer V pyramidal neurons, resting membrane potential became more negative, membrane input resistance (R_{in}) decreased and capacitance (C_{in}) increased during the first postnatal week, which is well agreement with previous studies (Zhang, 2004;Christophe et al., 2005). Moreover, their action potential amplitude increased and duration decreased with increase of age during the first postnatal week in accordance with other studies performed on supragranular pyramidal neurons and layer V pyramidal neurons of visual, sensorimotor, and prefrontal areas of rodent neocortex (Mccormick and Prince, 1987;Franceschetti et al., 1998;Zhu, 2000;Zhang, 2004;Christophe et al., 2005). The active and passive membrane properties of subplate neurons were similar to those reported previously (Friauf et al., 1990;Luhmann et al., 2000;Hanganu et al., 2001). When depolarized by intracellular current injection, subplate neurons were capable of firing overshooting, repetive and relatively high frequencies action potentials. During the first postnatal week, the AP amplitude as well as capacitance (C_{in}) increased, however, membrane input resistance (R_{in}) and duration of AP decreased with increase of age. For GABAergic interneurons, we found that R_{in} decreased and C_{in} increased during the first 2 postnatal weeks. While the C_{in} increase reflects an enlargement of the dendritic arbor (Doischer et al., 2008), both the enlarged membrane surface as well as the enhanced expression of two pore K^+ channels (Okaty et al., 2009) can contribute to the substantial decrease in R_{in}. Second, during this period, GABAergic interneurons showed a profound acceleration of AP discharges and a shortening of action

potentials with increase of age. Although the observed maximal discharge frequencies are lower than the discharge frequencies in adult fast-spiking interneurons (Connors and Gutnick, 1990), they are comparable to the discharge frequencies reported for immature GABAergic interneurons (Doischer et al., 2008;Okaty et al., 2009) and are considerably higher than the discharge frequencies of immature neocortical pyramidal neurons (Mccormick and Prince, 1987;Luhmann et al., 2000;Bahrey and Moody, 2003). However, in contrast to a previous report on fast-spiking neocortical interneurons (Okaty et al., 2009), we found that already in the P6-9 age group all interneurons showed virtually no spike adaptation. All these developmental changes serve to adapt interneurons to fast signaling (Doischer et al., 2008). A further classification of the GAD67-GFP labeled interneurons, e.g. regarding their molecular phenotype or their axonal and dendritic projections (Markram et al., 2004;Ascoli et al., 2008), is hindered by the delayed expression of molecular markers (Delecea et al., 1995;Erickson and Lewis, 2002;Itami et al., 2007) and the ongoing maturation of morphological and electrophysiological properties of the GABAergic system that continues to develop until adolescence (Okaty et al., 2009;Sauer and Bartos, 2011;Kilb, 2012).

4.2 Resonance properties of different neuronal populations

We showed in this study that for all neuronal cell types (Cajal-Retzius cells, supragranular pyramidal neurons, layer V pyramidal neurons, subplate neurons and GABAergic interneurons) the average resonance frequency was rather low in the delta frequency range. “In juvenile to adult neocortical neurons subthreshold resonance with similar properties has been observed. In the rat sensorimotor cortex ~58% of the regular spiking neurons showed resonance with a resonance strength of 1.4±1.3 at a frequency of 1.3±1.4 Hz (Hutcheon et al., 1996). A comparable low resonance frequency has also be observed for dendritic resonance in layer V pyramidal cell (Ulrich, 2002), while a slightly higher resonance at ~5 Hz was found in the frontal cortex of adult guinea pigs (Gutfreund et al., 1995). Our observation

that not all neurons showed subthreshold resonance is a clear indication that a low-frequency resonance is not an innate membrane property of immature neurons. This observation also raises the question, whether resonant and non-resonant neurons participate to different neuronal networks or process different functional roles within the immature neocortex. Cajal-Retzius neurons showed reliable subthreshold resonance in all investigated cells, which corresponds to the homogenous membrane properties observed for different Cajal-Retzius cell subtypes (Sava et al., 2010). The resonance frequencies of GABAergic interneurons in this study are considerably different from the rather high resonance frequencies of up to 50 Hz observed in hippocampal fast spiking basket cells (Pike et al., 2000), but comparable to other types of interneurons with subthreshold resonance in the delta to theta frequency range (Solinas et al., 2007;Zemankovics et al., 2010;Boehlen et al., 2011;van Brederode and Berger, 2011). A comparable low resonance frequency and strength has also been reported for pyramidal neurons in the adult (Hutcheon et al., 1996;Ulrich, 2002) and immature neocortex (Sun et al., 2012).

4.3 Leak conductance may influence the resonance properties of neurons.

Tight-seal whole-cell recordings induce an additional leak conductance via the seal between the membrane and the pipette, which may influence the resting membrane potential (Sava et al., 2010). In our recordings this error accounts for a slight depolarization, thus under "undisturbed" conditions the resting membrane potentials most probably is between -63 and -82 mV (**Table 1**). In Cajal-Retzius cells and supragranular pyramidal neurons the resonance frequency was not affected by a shift in the holding potential to -86 mV. But in Cajal-Retzius cells and GABAergic interneurons a more hyperpolarized resting membrane potential attenuated the resonance strength. In contrast, in layer V pyramidal cells the resonance frequency was voltage-dependent, thus in these neurons the resonance frequency may be slightly underestimated under our recording conditions. Furthermore, the artificial leak conductance introduced by the seal reduces the apparent input resistance of the

cell. Since the input resistance is an essential element of resonant circuits (Hutcheon et al., 1996), this leak conductance influences the resonance properties of the recorded neurons. Theoretically such a parallel leak resistance attenuates the amplitude of voltage responses and reduces the resonance frequency (Newell and Schlichter, 2005), which will cause an underestimation of resonance strength and amplitude under our recording conditions.

4.4 Mechanisms of subthreshold resonance

Subthreshold resonance arises from interactions of membrane resistance, capacitance and inductive elements in a parallel configuration. The inductive elements responsible for the generation of membrane resonance can be generated by voltage-dependent conductances with an activation kinetic that is larger than the membrane time constant (Hutcheon and Yarom, 2000). The passive membrane properties capacitance and resistance are determined by the surface of the plasma membrane and by leak conductances and establish the low-pass filtering characteristic innate to all neurons (Barrett and Crill, 1974). The inductive elements responsible for the "high-pass" elements underlying membrane resonance can be generated by voltage-dependent conductances with an activation kinetic that is larger than the membrane time constant (Hutcheon and Yarom, 2000). In particular I_h, persistent Na^+ currents, t-type Ca^{2+} and m-type K^+ currents have been suggested to underlie the inductive element of membrane resonance (Puil et al., 1994;Hutcheon et al., 1996;Pape and Driesang, 1998;Hu et al., 2002;Zemankovics et al., 2010). Interestingly, we found that there is no common mechanism underlying membrane resonance in immature neocortical neurons. One important ionic current that is frequently involved in subthreshold resonance is the I_h (Hutcheon et al., 1996;Pape, 1996). I_h is expressed in different neuronal types (Berger et al., 2001;Hu et al., 2002;Wang et al., 2006;Aponte et al., 2006;Zemankovics et al., 2010;Heys et al., 2010) and has been shown to be essential for the generation of subthreshold resonance in different classes of neurons (Berger et al., 2001;Hu et al., 2002;Wang et

al., 2006;Zemankovics et al., 2010;Heys et al., 2010). In Cajal-Retzius cells and layer V pyramidal neurons inhibition of I_h by ZD7288 virtually abolished subthreshold resonance, indicating that in these neuronal cell types subthreshold resonance is mainly mediated by I_h (Zemankovics et al., 2010). While we observed an I_h in immature GABAergic interneurons and layer II/III pyramidal neurons, blockade of this current did not affect subthreshold resonance. This finding suggests that I_h is most probably not directly involved in the generation of subthreshold resonance in immature GABAergic interneurons and layer II/III pyramidal neurons. Although this result is in discrepancy with observations in mature hippocampal interneuron (Zemankovics et al., 2010), it has already been shown for adult GABAergic interneurons that even high densities of I_h did not necessarily generate resonant membrane properties (Anderson et al., 2011).

Another ionic current that is frequently involved in subthreshold resonance is the t-type Ca^{2+} currents (Ertel and Ertel, 1997). In immature layer II/III pyramidal neurons, the subthreshold resonance was significantly reduced by 1 mM of Ni^{2+}, suggesting that t-type Ca^{2+} channels may mediate resonance in this neuronal population (Puil et al., 1994). In GABAergic interneurons I demonstrated that subthreshold resonance was effectively abolished in the presence of Ni^{2+}, a relatively selective blocker of t-type Ca^{2+} currents (Ertel and Ertel, 1997). This result strongly suggests that also in immature neocortical interneurons a t-type Ca^{2+} current is essential for the occurrence of subthreshold resonance.

In addition to the t-type Ca^{2+} current, I_{NaP} is also involved in subthreshold resonance (Hutcheon and Yarom, 2000;Hu et al., 2002). My results demonstrate that at holding potential of –66 mV the blockade of I_{NaP} abolished subthreshold resonance in GABAergic interneurons, suggesting that I_{NaP} is essential for subthreshold resonance under this condition. In contrast, at a more hyperpolarized potential of –86 mV inhibition of I_{NaP} had no significant effect on subthreshold resonance, suggesting that it is not activated and does thus not contribute to subthreshold potential under

this condition. This suggestion is in accordance with my observation, that subthreshold resonance is attenuated at more hyperpolarized potentials and indicate that I_{NaP} amplifies the voltage deflections generated by t-type Ca^{2+} currents under this condition (Hutcheon and Yarom, 2000). On the other hand the complete suppression of subthreshold resonance at –66 mV by either Ni^{2+} or TTX indicated that under this condition a more complex interaction between both ion currents must occur. In cerebellar interneurons (Solinas et al., 2007) and hippocampal stratum radiatum interneurons (Boehlen et al., 2011) I_{NaP} also contributes to the generation of subthreshold resonance, although in the latter a contribution of I_h could not be excluded.

4.5 Subthreshold resonance increases the cutoff frequency of the immature neurons.

One striking observation was that the subthreshold resonance drastically increases the cutoff frequency of the immature neurons. Blocking of I_h in Cajal-Retzius cells and layer V neurons not only attenuated subthreshold resonance, but also substantially reduced the cutoff frequency. Due to the relatively high input resistance of immature neurons, these cells have a rather slow time constant (Luhmann et al., 2000;Hanganu et al., 2001;Hirsch and Luhmann, 2008), resulting in rather low cutoff frequencies. The slow membrane time constant in combination with the longer decay times of EPSCs at immature synapses contribute to an enhanced temporal summation of immature neurons (Etherington and Williams, 2011). My results demonstrate that addition of the inductive, voltage-dependent component I_h not only led to the appearance of resonance, but also affected the cutoff frequency. This resonance-related increase of the cutoff frequency will increase temporal fidelity and reduce the temporal summation of synaptic inputs. It has recently been suggested for CA1 neurons that the effect of I_h on temporal integration of excitatory and inhibitory postsynaptic potentials (Berger et al., 2001), rather than its contribution to membrane resonance, underlies the facilitation of spike-time

precision mediated by I_h (Gastrein et al., 2011).” (from Sun et al., 2012).

4.6 Resonance properties of single neurons may contribute to the low frequency of oscillatory patterns in the early neuronal networks

Oscillatory activity is not only a hallmark of mature neuronal circuits (Buzsaki and Draguhn, 2004), but can also be observed in the developing neocortex (Khazipov and Luhmann, 2006). EEG recordings from preterm infants revealed delta brush patterns, which consist of 0.3-1.5 Hz delta waves underlying a 8-25 Hz spindle like oscillations (Khazipov and Luhmann, 2006). In neonatal rodents, comparable spontaneous activity transients were found in the primary visual cortex before eye opening (Colonnese et al., 2010;Colonnese and Khazipov, 2010). Moreover, in the immature primary somatosensory cortex evoked and spontaneous oscillations ranging from alpha to gamma frequency band can be observed *in-vivo* (Khazipov et al., 2004;Yang et al., 2009;Minlebaev et al., 2011). Stimulation of the neocortical network *in-vitro* with carbachol or glutamate also induced reliable transient alpha to beta band oscillations (Kilb and Luhmann, 2003;Wagner and Luhmann, 2006) that are triggered by subplate cells and involve supragranular pyramidal neurons (Dupont et al., 2006). It has been proposed that resonance properties of single neurons can contribute to the oscillatory behavior of neuronal networks (Hutcheon and Yarom, 2000).

The present study clearly demonstrate that subplate cells and supragrannular neurons, but also layer V pyramidal neurons and GABAergic interneurons, show resonance at rather low frequencies between 0.8 and 2.0 Hz, although the resonance frequencies may be higher under *in-vivo* conditions. Because subthreshold oscillations reveal a strong temperature dependency with a Q10 of about 4 (Hu et al., 2002). Under consideration of this temperature dependency the observed resonance frequencies correspond to frequencies between 4 and 6 Hz under in-vivo conditions (about 38 ° C in rats). The resonance properties of these neurons may support the

generation of low frequency activity patterns like delta brushes or spontaneous activity transients (Colonnese et al., 2010;Colonnese and Khazipov, 2010). On the other hand, the intrinsic resonance frequency of these neurons is below the alpha to gamma frequency range observed for spontaneous and evoked spindle activity *in-vivo* (Khazipov et al., 2004;Yang et al., 2009) or for the transient *in-vitro* network oscillations (Dupont et al., 2006;Wagner and Luhmann, 2006). Cajal-Retzius cells showed a slightly higher resonance frequency of 2.4-2.9 Hz, which may correspond to a frequency of ~10 Hz under *in-vivo* conditions and may thus relate to the frequency of spindle-bursts (Khazipov et al., 2004;Yang et al., 2009).

4.7 Resonance behaviors of single neurons may contribute to synaptic filtering

Besides generating oscillatory behavior, subthreshold resonance also tunes neurons to specific synaptic inputs (Izhikevich, 2002). For example, I_h currents in the dendritic compartment of adult pyramidal neurons generate subthreshold resonance in the theta frequency range and thereby tune dendritic filtering of synaptic inputs to this frequency range (Ulrich, 2002). The low resonance frequency observed for all neurons investigated in the present study suggests that these neurons most probably are not directly tuned to spindle bursts or the alpha to gamma band oscillations. The frequency of excitatory and GABAergic synaptic inputs recorded under patch-clamp conditions in the immature cortex *in-vivo* is mainly locked to spindle busts (Khazipov et al., 2004;Hanganu et al., 2006;Minlebaev et al., 2011), while subthreshold resonance in immature GABAergic interneurons was in the delta band, which suggests that interneurons are most probably not directly tuned to such synaptic inputs. Therefore I propose that in the immature neocortex these neuronal populations are not frequency tuned to spindle bursts or alpha to gamma band oscillations but may support the generation of low frequency activity patterns like delta brushes or spontaneous activity transients.

5. Summary

Subthreshold resonance is a characteristic membrane property of different neuronal classes, is critically involved in the generation of network oscillations, and tunes the integration of synaptic inputs to particular frequency ranges. In order to investigate whether resonance properties of distinct neuronal populations in the immature neocortex contribute to these network oscillations, I performed whole-cell patch-clamp recordings from visually identified neurons in tangential and coronal neocortical slices from postnatal day (P) P0-P7 C57Bl/6 and P6-P13 GAD67-GFP knock-in mice. Subthreshold resonance was analyzed by sinusoidal current injection of varying frequency. All Cajal-Retzius cells showed subthreshold resonance with an average frequency of 2.6 ± 0.1 Hz (n=60), which was massively reduced by ZD7288, a blocker of hyperpolarization-activated cation currents. About 65.6% (n=61) of the supragranular pyramidal neurons showed subthreshold resonance with an average frequency of 1.4 ± 0.1 Hz (n=40). Application of 1 mM Ni^{2+} suppressed subthreshold resonance, suggesting that low-threshold Ca^{2+} currents contribute to resonance in these neurons. About 63.6% (n=77) of the layer V pyramidal neurons showed subthreshold resonance with an average frequency of 1.4 ± 0.2 Hz (n=49), which was abolished by ZD7288. Only 44.1% (n=59) of the subplate neurons showed subthreshold resonance with an average frequency of 1.3 ± 0.2 Hz (n=26) and a small resonance strength. Finally, 50% of the investigated GABAergic interneurons showed subthreshold resonance with an average frequency of 2.0 ± 0.2 Hz (*n*=42). Membrane hyperpolarization to –86 mV attenuated the frequency and strength of subthreshold resonance. Subthreshold resonance was virtually abolished in the presence of 1 mM Ni^{2+}, suggesting that t-type Ca^{2+} currents are critically involved in the generation of resonance, while ZD7288 had no effect. Application of 0.4 µM TTX suppressed subthreshold resonance at depolarized, but not hyperpolarized membrane potential, suggesting that persistent Na^{+} current contribute to the amplification of membrane resonance.

In summary, these results demonstrate that all investigated neuronal subpopulations reveal resonance behavior, with either hyperpolarization-activated cation or low-threshold Ca^{2+} currents contributing to the subthreshold resonance. GABAergic interneurons also express subthreshold resonance at low frequencies, with t-type Ca^{2+} and persistent Na^{+} currents underlying the generation of membrane resonance. The membrane resonance of immature neurons may contribute to the generation of slow oscillatory activity pattern in the immature neocortex and enhance the temporal precision of synaptic integration in developing cortical neurons.

Reference List

Achilles K, Okabe A, Ikeda M, Shimizu-Okabe C, Yamada J, Fukuda A, Luhmann HJ, Kilb W (2007) Kinetic properties of Cl- uptake mediated by Na+-dependent K+-2Cl(-) cotransport in immature rat neocortical neurons. J Neurosci 27: 8616-8627.

Allendoerfer KL, Shatz CJ (1994) The Subplate, A Transient Neocortical Structure - Its Role in the Development of Connections Between Thalamus and Cortex. Annual Review of Neuroscience 17: 185-218.

Anderson CM, Torres F, Faoro A (1985) The Eeg of the Early Premature. Electroencephalography and Clinical Neurophysiology 60: 95-105.

Anderson WD, Galvan EJ, Mauna JC, Thiels E, Barrionuevo G (2011) Properties and functional implications of I-h in hippocampal area CA3 interneurons. Pflugers Archiv-European Journal of Physiology 462: 895-912.

Aponte Y, Lien CC, Reisinger E, Jonas P (2006) Hyperpolarization-activated cation channels in fast-spiking interneurons of rat hippocampus. Journal of Physiology-London 574: 229-243.

Ascoli GA, Alonso-Nanclares L, Anderson SA, Barrionuevo G, Benavides-Piccione R, Burkhalter A, Buzsaki G, Cauli B, DeFelipe J, Fairen A, Feldmeyer D, Fishell G, Fregnac Y, Freund TF, Gardner D, Gardner EP, Goldberg JH, Helmstaedter M, Hestrin S, Karube F, Kisvarday ZF, Lambolez B, Lewis DA, Marin O, Markram H, Munoz A, Packer A, Petersen CCH, Rockland KS, Rossier J, Rudy B, Somogyi P, Staiger JF, Tamas G, Thomson AM, Toledo-Rodriguez M, Wang Y, West DC, Yuste R (2008) Petilla terminology: nomenclature of features of GABAergic interneurons of the cerebral cortex. Nat Rev Neurosci 9: 557-568.

Bahrey HLP, Moody WJ (2003) Early development of voltage-gated ion currents and

firing properties in neurons of the mouse cerebral cortex. Journal of Neurophysiology 89: 1761-1773.

Baker SN (2007) Oscillatory interactions between sensorimotor cortex and the periphery. Current Opinion in Neurobiology 17: 649-655.

Bar I, de Rouvroit CL, Goffinet AM (2000) The evolution of cortical development. An hypothesis based on the role of the Reelin signaling pathway. Trends in Neurosciences 23: 633-638.

Barrett JN, Crill WE (1974) Specific Membrane Properties of Cat Motoneurons. Journal of Physiology-London 239: 301-&.

Baumeister J, Barthel T, Geiss KR, Weiss M (2008) Influence of phosphatidylserine on cognitive performance and cortical activity after induced stress. Nutritional Neuroscience 11: 103-110.

Berger T, Larkum ME, Luscher HR (2001) High I-h channel density in the distal apical dendrite of layer V pyramidal cells increases bidirectional attenuation of EPSPs. Journal of Neurophysiology 85: 855-868.

Bielle F, Griveau A, Narboux-Neme N, Vigneau S, Sigrist M, Arber S, Wassef M, Pierani A (2005) Multiple origins of Cajal-Retzius cells at the borders of the developing pallium. Nature Neuroscience 8: 1002-1012.

Bland BH (1986) The Physiology and Pharmacology of Hippocampal-Formation Theta Rhythms. Progress in Neurobiology 26: 1-54.

Boehlen A, Heinemann U, Henneberger C (2011) Heterogeneous Voltage Dependence of Interneuron Resonance in the Hippocampal Stratum Radiatum of Adult Rats. Synapse 65: 1378-1381.

Braak H, Braak E (1976) The pyramidal cells of Betz within the cingulate and precentral gigantopyramidal field in the human brain. A Golgi and

pigmentarchitectonic study. Cell Tissue Res 172: 103-119.

Brockmann MD, Poschel B, Cichon N, Hanganu-Opatz IL (2011) Coupled Oscillations Mediate Directed Interactions between Prefrontal Cortex and Hippocampus of the Neonatal Rat. Neuron 71: 332-347.

Brown DA, Adams PR (1980) Muscarinic Suppression of A Novel Voltage-Sensitive K+ Current in A Vertebrate Neuron. Nature 283: 673-676.

Brown DA, Gahwiler BH, Griffith WH, Halliwell JV (1990) Membrane Currents in Hippocampal-Neurons. Progress in Brain Research 83: 141-160.

Buzsaki G (2002) Theta oscillations in the hippocampus. Neuron 33: 325-340.

Buzsaki G (2006) Rhythms of the brain. Oxford University Express.

Buzsaki G, Draguhn A (2004) Neuronal oscillations in cortical networks. Science 304: 1926-1929.

Buzsaki G, Wang XJ (2012) Mechanisms of Gamma Oscillations. Annual Review of Neuroscience, Vol 35 35: 203-225.

Cang JH, Renteria RC, Kaneko M, Liu XR, Copenhagen DR, Stryker MP (2005) Development of precise maps in visual cortex requires patterned spontaneous activity in the retina. Neuron 48: 797-809.

Chandrasekaran AR, Plas DT, Gonzalez E, Crair MC (2005) Evidence for an instructive role of retinal activity in retinotopic map refinement in the superior colliculus of the mouse. J Neurosci 25: 6929-6938.

Christophe E, Doerflinger N, Lavery DJ, Molnar Z, Charpak S, Audinat E (2005) Two Populations of layer V pyramidal cells of the mouse neocortex: Development and sensitivity to anesthetics. Journal of Neurophysiology 94: 3357-3367.

Colonnese MT, Kaminska A, Minlebaev M, Milh M, Bloem B, Lescure S, Moriette G,

Chiron C, Ben Ari Y, Khazipov R (2010) A Conserved Switch in Sensory Processing Prepares Developing Neocortex for Vision. Neuron 67: 480-498.

Colonnese MT, Khazipov R (2010) "Slow Activity Transients" in Infant Rat Visual Cortex: A Spreading Synchronous Oscillation Patterned by Retinal Waves (vol 30, pg 4325, 2010). J Neurosci 30: 6170.

Connors BW, Gutnick MJ (1990) Intrinsic Firing Patterns of Diverse Neocortical Neurons. Trends in Neurosciences 13: 99-104.

Crill WE (1996) Persistent sodium current in mammalian central neurons. Annual Review of Physiology 58: 349-362.

de Kock CPJ, Bruno RM, Spors H, Sakmann B (2007) Layer- and cell-type-specific suprathreshold stimulus representation in rat primary somatosensory cortex. Journal of Physiology-London 581: 139-154.

Delecea L, Delrio JA, Soriano E (1995) Developmental Expression of Parvalbumin Messenger-Rna in the Cerebral-Cortex and Hippocampus of the Rat. Molecular Brain Research 32: 1-13.

Diamond ME, Huang W, Ebner FF (1994) Laminar Comparison of Somatosensory Cortical Plasticity. Science 265: 1885-1888.

Doischer D, Hosp JA, Yanagawa Y, Obata K, Jonas P, Vida I, Bartos M (2008) Postnatal Differentiation of Basket Cells from Slow to Fast Signaling Devices. J Neurosci 28: 12956-12968.

Dumitriu D, Cossart R, Huang J, Yuste R (2007) Correlation between axonal morphologies and synaptic input kinetics of interneurons from mouse visual cortex. Cerebral Cortex 17: 81-91.

Dupont E, Hanganu IL, Kilb W, Hirsch S, Luhmann HJ (2006) Rapid developmental switch in the mechanisms driving early cortical columnar networks. Nature 439:

79-83.

Engel AK, Fries P, Singer W (2001) Dynamic predictions: Oscillations and synchrony in top-down processing. Nat Rev Neurosci 2: 704-716.

Erchova I, Kreck G, Heinemann U, Herz AVM (2004) Dynamics of rat entorhinal cortex layer II and III cells: characteristics of membrane potential resonance at rest predict oscillation properties near threshold. Journal of Physiology-London 560: 89-110.

Erickson SL, Lewis DA (2002) Postnatal development of parvalbumin- and GABA transporter-immunoreactive axon terminals in monkey prefrontal cortex. Journal of Comparative Neurology 448: 186-202.

Ertel SI, Ertel EA (1997) Low-voltage-activated T-type Ca2+ channels. Trends in Pharmacological Sciences 18: 37-42.

Etherington SJ, Williams SR (2011) Postnatal Development of Intrinsic and Synaptic Properties Transforms Signaling in the Layer 5 Excitatory Neural Network of the Visual Cortex. J Neurosci 31: 9526-9537.

Feldmeyer D, Roth A, Sakmann B (2005) Monosynaptic connections between pairs of spiny stellate cells in layer 4 and pyramidal cells in layer 5A indicate that lemniscal and paralemniscal afferent pathways converge in the infragranular somatosensory cortex. J Neurosci 25: 3423-3431.

Fox K (2002) Anatomical pathways and molecular mechanisms for plasticity in the barrel cortex. Neuroscience 111: 799-814.

Franceschetti S, Sancini G, Panzica F, Radici C, Avanzini G (1998) Postnatal differentiation of firing properties and morphological characteristics in layer V pyramidal neurons of the sensorimotor cortex. Neuroscience 83: 1013-1024.

French CR, Gage PW (1985) A Threshold Sodium Current in Pyramidal Cells in Rat

Hippocampus. Neuroscience Letters 56: 289-293.

Friauf E, Mcconnell SK, Shatz CJ (1990) Functional Synaptic Circuits in the Subplate During Fetal and Early Postnatal-Development of Cat Visual-Cortex. J Neurosci 10: 2601-2613.

Friedlander MJ, Torres-Reveron J (2009) The changing roles of neurons in the cortical subplate. Frontiers in Neuroanatomy 3.

Gabriele ML, Brunso-Bechtold JK, Henkel CK (2000) Plasticity in the development of afferent patterns in the inferior colliculus of the rat after unilateral cochlear ablation. J Neurosci 20: 6939-6949.

Gastrein P, Campanac E, Gasselin C, Cudmore RH, Bialowas A, Carlier E, Fronzaroli-Molinieres L, Ankri N, Debanne D (2011) The role of hyperpolarization-activated cationic current in spike-time precision and intrinsic resonance in cortical neurons in vitro. Journal of Physiology-London 589: 3753-3773.

Ghosh A, Shatz CJ (1992) Involvement of Subplate Neurons in the Formation of Ocular Dominance Columns. Science 255: 1441-1443.

Gold I (1999) Does 40-Hz oscillation play a role in visual consciousness? Consciousness and Cognition 8: 186-195.

GoldmanRakic PS (1996) Regional and cellular fractionation of working memory. Proceedings of the National Academy of Sciences of the United States of America 93: 13473-13480.

Grant E, Hoerder-Suabedissen A, Molnar Z (2012) Development of the corticothalamic projections. Front Neurosci 6: 53.

Griveau A, Borello U, Causeret F, Tissir F, Boggetto N, Karaz S, Pierani A (2010) A Novel Role for Dbx1-Derived Cajal-Retzius Cells in Early Regionalization of the

Cerebral Cortical Neuroepithelium. Plos Biology 8.

Gutfreund Y, Yarom Y, Segev I (1995) Subthreshold Oscillations and Resonant-Frequency in Guinea-Pig Cortical-Neurons - Physiology and Modeling. Journal of Physiology-London 483: 621-640.

Haas JS, White JA (2002) Frequency selectivity of layer II stellate cells in the medial entorhinal cortex. Journal of Neurophysiology 88: 2422-2429.

Halliwell JV, Adams PR (1982) Voltage-Clamp Analysis of Muscarinic Excitation in Hippocampal-Neurons. Brain Research 250: 71-92.

Hanganu IL, Ben Ari Y, Khazipov R (2006) Retinal waves trigger spindle bursts in the neonatal rat visual cortex. J Neurosci 26: 6728-6736.

Hanganu IL, Kilb W, Luhmann HJ (2001) Spontaneous synaptic activity of subplate neurons in neonatal rat somatosensory cortex. Cerebral Cortex 11: 400-410.

Hanganu IL, Kilb W, Luhmann HJ (2002) Functional synaptic projections onto subplate neurons in neonatal rat somatosensory cortex. J Neurosci 22: 7165-7176.

Hanganu-Opatz IL (2010) Between molecules and experience: Role of early patterns of coordinated activity for the development of cortical maps and sensory abilities. Brain Research Reviews 64: 160-176.

Hans Berger (1929) Ueber das Elektroenkephalogramm des Menschen. Arch f Psychiatr 87: 527-570.

Harris JA, Miniussi C, Harris IM, Diamond ME (2002) Transient storage of a tactile memory trace in primary somatosensory cortex. J Neurosci 22: 8720-8725.

Hasselmo ME (2005) What is the function of hippocampal theta Rhythm? Linking behavioral data to phasic properties of field potential and unit recording data. Hippocampus 15: 936-949.

Hestrin S, Armstrong WE (1996) Morphology and physiology of cortical neurons in layer I. J Neurosci 16: 5290-5300.

Heys JG, Giocomo LM, Hasselmo ME (2010) Cholinergic Modulation of the Resonance Properties of Stellate Cells in Layer II of Medial Entorhinal Cortex. Journal of Neurophysiology 104: 258-270.

Hirsch S, Luhmann HJ (2008) Pathway-specificity in N-methyl-D-aspartate receptor-mediated synaptic inputs onto subplate neurons. Neuroscience 153: 1092-1102.

Holmes GL, Lombroso CT (1993) Prognostic Value of Background Patterns in the Neonatal Eeg. Journal of Clinical Neurophysiology 10: 323-352.

Hu H, Vervaeke K, Graham LJ, Storm JF (2009) Complementary Theta Resonance Filtering by Two Spatially Segregated Mechanisms in CA1 Hippocampal Pyramidal Neurons. J Neurosci 29: 14472-14483.

Hu H, Vervaeke K, Storm JF (2002) Two forms of electrical resonance at theta frequencies, generated by M-current, h-current and persistent Na+ current in rat hippocampal pyramidal cells. Journal of Physiology-London 545: 783-805.

Huang W, Armstrong-James M, Rema V, Diamond ME, Ebner FF (1998) Contribution of supragranular layers to sensory processing and plasticity in adult rat barrel cortex. Journal of Neurophysiology 80: 3261-3271.

Huerta PT, Lisman JE (1993) Heightened Synaptic Plasticity of Hippocampal Ca1 Neurons During A Cholinergically Induced Rhythmic State. Nature 364: 723-725.

Hughes JR (2008) Gamma, fast, and ultrafast waves of the brain: Their relationships with epilepsy and behavior. Epilepsy & Behavior 13: 25-31.

Huguenard JR (1996) Low-threshold calcium currents in central nervous system neurons. Annual Review of Physiology 58: 329-348.

Hutcheon B, Miura RM, Puil E (1996) Subthreshold membrane resonance in neocortical neurons. Journal of Neurophysiology 76: 683-697.

Hutcheon B, Miura RM, Yarom Y, Puil E (1994) Low-Threshold Calcium Current and Resonance in Thalamic Neurons - A Model of Frequency Preference. Journal of Neurophysiology 71: 583-594.

Hutcheon B, Yarom Y (2000) Resonance, oscillation and the intrinsic frequency preferences of neurons. Trends in Neurosciences 23: 216-222.

Itami C, Kimura F, Nakamura S (2007) Brain-derived neurotrophic factor regulates the maturation of layer 4 fast-spiking cells after the second postnatal week in the developing barrel cortex. J Neurosci 27: 2241-2252.

Izhikevich EM (2002) Resonance and selective communication via bursts in neurons having subthreshold oscillations. Biosystems 67: 95-102.

Izhikevich EM, Desai NS, Walcott EC, Hoppensteadt FC (2003) Bursts as a unit of neural information: selective communication via resonance. Trends in Neurosciences 26: 161-167.

Jentsch TJ (2000) Neuronal KCNQ potassium channels: Physiology and role in disease. Nat Rev Neurosci 1: 21-30.

Kahana MJ, Seelig D, Madsen JR (2001) Theta returns. Current Opinion in Neurobiology 11: 739-744.

Kandler K (2004) Activity-dependent organization of inhibitory circuits: lessons from the auditory system. Current Opinion in Neurobiology 14: 96-104.

Kanold PO (2009) Subplate neurons: crucial regulators of cortical development and plasticity. Frontiers in Neuroanatomy 3.

Kanold PO, Kara P, Reid RC, Shatz CJ (2003) Role of subplate neurons in functional

maturation of visual cortical columns. Science 301: 521-525.

Kanold PO, Luhmann HJ (2010) The Subplate and Early Cortical Circuits. Annual Review of Neuroscience, Vol 33 33: 23-48.

Kanold PO, Shatz CJ (2006) Subplate neurons regulate maturation of cortical inhibition and outcome of ocular dominance plasticity. Neuron 51: 627-638.

Khazipov R, Luhmann HJ (2006) Early patterns of electrical activity in the developing cerebral cortex of humans and rodents. Trends in Neurosciences 29: 414-418.

Khazipov R, Sirota A, Leinekugel X, Holmes GL, Ben Arf Y, Buzsaki G (2004) Early motor activity drives spindle bursts in the developing somatosensory cortex. Nature 432: 758-761.

Kilb W (2012) Development of the GABAergic System from Birth to Adolescence. Neuroscientist 18: 613-630.

Kilb W, Kirischuk S, Luhmann HJ (2011) Electrical activity patterns and the functional maturation of the neocortex. Eur J Neurosci 34: 1677-1686.

Kilb W, Luhmann HJ (2000) Characterization of a hyperpolarization-activated inward current in Cajal-Retzius cells in rat neonatal neocortex. Journal of Neurophysiology 84: 1681-1691.

Kilb W, Luhmann HJ (2001) Spontaneous GABAergic postsynaptic currents in Cajal-Retzius cells in neonatal rat cerebral cortex. Eur J Neurosci 13: 1387-1390.

Kilb W, Luhmann HJ (2003) Carbachol-induced network oscillations in the intact cerebral cortex of the newborn rat. Cerebral Cortex 13: 409-421.

Kim HG, Fox K, Connors BW (1995) Properties of Excitatory Synaptic Events in Neurons of Primary Somatosensory Cortex of Neonatal Rats. Cerebral Cortex 5:

148-157.

Klink R, Alonso A (1993) Ionic Mechanisms for the Subthreshold Oscillations and Differential Electroresponsiveness of Medial Entorhinal Cortex Layer-Ii Neurons. Journal of Neurophysiology 70: 144-157.

Kolev V, Basar-Eroglu C, Aksu F, Basar E (1994) EEG rhythmicities evoked by visual stimuli in three-year-old children. Int J Neurosci 75: 257-270.

Lalo E, Gilbertson T, Doyle L, Di Lazzaro V, Cioni B, Brown P (2007) Phasic increases in cortical beta activity are associated with alterations in sensory processing in the human. Experimental Brain Research 177: 137-145.

Lamblin MD, Andre M, Challamel MJ, Curzi-Dascalova L, d'Allest AM, De Giovanni E, Moussalli-Salefranque F, Navelet Y, Plouin P, Radvanyi-Bouvet MF, Samson-Dollfus D, Vecchierini-Blineau MF (1999) [Electroencephalography of the premature and term newborn. Maturational aspects and glossary]. Neurophysiol Clin 29: 123-219.

Lampl I, Yarom Y (1997) Subthreshold oscillations and resonant behavior: Two manifestations of the same mechanism. Neuroscience 78: 325-341.

Leake PA, Hradek GT, Chair L, Snyder RL (2006) Neonatal deafness results in degraded topographic specificity of auditory nerve projections to the cochlear nucleus in cats. Journal of Comparative Neurology 497: 13-31.

Leao RN, Sun H, Svahn K, Berntson A, Youssoufian M, Paolini AG, Fyffe REW, Walmsley B (2006) Topographic organization in the auditory brainstem of juvenile mice is disrupted in congenital deafness. Journal of Physiology-London 571: 563-578.

Lee J, Kim D, Shin HS (2004) Lack of delta waves and sleep disturbances during non-rapid eye movement sleep in mice lacking alpha 1(G)-subunit of T-type calcium

channels. Proceedings of the National Academy of Sciences of the United States of America 101: 18195-18199.

Lemon RN (2008) Descending pathways in motor control. Annual Review of Neuroscience 31: 195-218.

Leung LS, Yu HW (1998) Theta-frequency resonance in hippocampal CA1 neurons in vitro demonstrated by sinusoidal current injection. Journal of Neurophysiology 79: 1592-1596.

Luhmann HJ, Kilb W, Hanganu-Opatz IL (2009) Subplate cells: amplifiers of neuronal activity in the developing cerebral cortex. Frontiers in Neuroanatomy 3.

Luhmann HJ, Reiprich RA, Hanganu I, Kilb W (2000) Cellular physiology of the neonatal rat cerebral cortex: Intrinsic membrane properties, sodium and calcium currents. Journal of Neuroscience Research 62: 574-584.

Lund RD, Mustari MJ (1977) Development of the geniculocortical pathway in rats. J Comp Neurol 173: 289-306.

Luthi A, McCormick DA (1998) H-current: Properties of a neuronal and network pacemaker. Neuron 21: 9-12.

Maccaferri G, Mcbain CJ (1996) The hyperpolarization-activated current (I-h) and its contribution to pacemaker activity in rat CA1 hippocampal stratum oriens-alveus interneurones. Journal of Physiology-London 497: 119-130.

Machens CK, Romo R, Brody CD (2005) Flexible control of mutual inhibition: A neural model of two-interval discrimination. Science 307: 1121-1124.

Mann EO, Paulsen O (2007) Role of GABAergic inhibition in hippocampal network oscillations. Trends in Neurosciences 30: 343-349.

Maquet P, Degueldre C, Delfiore G, Aerts J, Peters JM, Luxen A, Franck G (1997)

Functional neuroanatomy of human slow wave sleep. J Neurosci 17: 2807-2812.

Markram H, Toledo-Rodriguez M, Wang Y, Gupta A, Silberberg G, Wu CZ (2004) Interneurons of the neocortical inhibitory system. Nat Rev Neurosci 5: 793-807.

Mccormick DA, Prince DA (1987) Postnatal-Development of Electrophysiological Properties of Rat Cerebral Cortical Pyramidal Neurons. Journal of Physiology-London 393: 743-762.

McLaughlin T, Torborg CL, Feller MB, O'Leary DDM (2003) Retinotopic map refinement requires spontaneous retinal waves during a brief critical period of development. Neuron 40: 1147-1160.

Megias M, Emri Z, Freund TF, Gulyas AI (2001) Total number and distribution of inhibitory and excitatory synapses on hippocampal CA1 pyramidal cells. Neuroscience 102: 527-540.

Meyer G, Goffinet AM, Fairen A (1999) Feature article what is a cajal-retzius cell? A reassessment of a classical cell type based on recent observations in the developing neocortex. Cerebral Cortex 9: 765-775.

Meyer G, Perez-Garcia CG, Abraham H, Caput D (2002) Expression of p73 and Reelin in the developing human cortex. J Neurosci 22: 4973-4986.

Minlebaev M, Colonnese M, Tsintsadze T, Sirota A, Khazipov R (2011) Early Gamma Oscillations Synchronize Developing Thalamus and Cortex. Science 334: 226-229.

Molnar Z, Adams R, Blakemore C (1998) Mechanisms underlying the early establishment of thalamocortical connections in the rat. J Neurosci 18: 5723-5745.

Neuhoff H, Neu A, Liss B, Roeper J (2002) I-h channels contribute to the different functional properties of identified dopaminergic subpopulations in the midbrain. J Neurosci 22: 1290-1302.

Newell EW, Schlichter LC (2005) Integration of K+ and Cl- currents regulate steady-state and dynamic membrane potentials in cultured rat microglia. Journal of Physiology-London 567: 869-890.

Okaty BW, Miller MN, Sugino K, Hempel CM, Nelson SB (2009) Transcriptional and Electrophysiological Maturation of Neocortical Fast-Spiking GABAergic Interneurons. J Neurosci 29: 7040-7052.

Pape HC (1996) Queer current and pacemaker: The hyperpolarization-activated cation current in neurons. Annual Review of Physiology 58: 299-327.

Pape HC, Driesang RB (1998) Ionic mechanisms of intrinsic oscillations in neurons of the basolateral amygdaloid complex. Journal of Neurophysiology 79: 217-226.

Perez-Reyes E, Cribbs LL, Daud A, Lacerda AE, Barclay J, Williamson MP, Fox M, Rees M, Lee JH (1998) Molecular characterization of a neuronal low-voltage-activated T-type calcium channel. Nature 391: 896-900.

Pike FG, Goddard RS, Suckling JM, Ganter P, Kasthuri N, Paulsen O (2000) Distinct frequency preferences of different types of rat hippocampal neurones in response to oscillatory input currents. Journal of Physiology-London 529: 205-213.

Puil E, Meiri H, Yarom Y (1994) Resonant Behavior and Frequency Preferences of Thalamic Neurons. Journal of Neurophysiology 71: 575-582.

Radnikow G, Feldmeyer D, Lubke J (2002) Axonal projection, input and output synapses, and synaptic physiology of Cajal-Retzius cells in the developing rat neocortex. J Neurosci 22: 6908-6919.

Raghavachari S, Kahana MJ, Rizzuto DS, Caplan JB, Kirschen MP, Bourgeois B, Madsen JR, Lisman JE (2001) Gating of human theta oscillations by a working memory task. J Neurosci 21: 3175-3183.

Rakic P (1977) Prenatal development of the visual system in rhesus monkey. Philos

Trans R Soc Lond B Biol Sci 278: 245-260.

Rakic P (1983) Geniculo-Cortical Connections in Primates - Normal and Experimentally Altered Development. Progress in Brain Research 58: 393-404.

Rubel EW, Fritzsch B (2002) Auditory system development: Primary auditory neurons and their targets. Annual Review of Neuroscience 25: 51-101.

Sarnthein J, Petsche H, Rappelsberger P, Shaw GL, von Stein A (1998) Synchronization between prefrontal and posterior association cortex during human working memory. Proceedings of the National Academy of Sciences of the United States of America 95: 7092-7096.

Sauer JF, Bartos M (2011) Postnatal differentiation of cortical interneuron signalling. Eur J Neurosci 34: 1687-1696.

Sava BA, David CS, Teissier A, Pierani A, Staiger JF, Luhmann HJ, Kilb W (2010) Electrophysiological and Morphological Properties of Cajal-Retzius Cells with Different Ontogenetic Origins. Neuroscience 167: 724-734.

Schubert D, Kotter R, Luhmann HJ, Staiger JF (2006) Morphology, electrophysiology and functional input connectivity of pyramidal neurons characterizes a genuine layer Va in the primary somatosensory cortex. Cerebral Cortex 16: 223-236.

Sejnowski TJ, Destexhe A (2000) Why do we sleep? Brain Research 886: 208-223.

Solinas S, Forti L, Cesana E, Mapelli J, De Schutter E, D'Angelo E (2007) Fast-reset of pacemaking and theta-frequency resonance patterns in cerebellar Golgi cells: Simulations of their impact in vivo. Frontiers in Cellular Neuroscience 1.

Soriano E, del Rio JA (2005) The cells of Cajal-Retzius: Still a mystery one century after. Neuron 46: 389-394.

Spruston N (2008) Pyramidal neurons: dendritic structure and synaptic integration. Nat Rev Neurosci 9: 206-221.

Stafstrom CE, Schwindt PC, Chubb MC, Crill WE (1985) Properties of persistent sodium conductance and calcium conductance of layer V neurons from cat sensorimotor cortex in vitro. J Neurophysiol 53: 153-170.

Storm JF (1990) Potassium Currents in Hippocampal Pyramidal Cells. Progress in Brain Research 83: 161-187.

Sun HY, Luhmann HJ, Kilb W (2012) Resonance properties of different neuronal populations in the immature mouse neocortex. Eur J Neurosci 36: 2753-2762.

Takiguchi-Hayashi K, Sekiguchi M, Ashigaki S, Takamatsu M, Hasegawa H, Suzuki-Migishima R, Yokoyama M, Nakanishi S, Tanabe Y (2004) Generation of reelin-positive marginal zone cells from the caudomedial wall of telencephalic vesicles. J Neurosci 24: 2286-2295.

Tamamaki N, Yanagawa Y, Tomioka R, Miyazaki JI, Obata K, Kaneko T (2003) Green fluorescent protein expression and colocalization with calretinin, parvalbumin, and somatostatin in the GAD67-GFP knock-in mouse. Journal of Comparative Neurology 467: 60-79.

Tecchio F, Zappasodi F, Porcaro C, Barbati G, Assenza G, Salustri C, Rossini PM (2008) High-gamma band activity of primary hand cortical areas: A sensorimotor feedback efficiency index. Neuroimage 40: 256-264.

Thut G, Miniussi C, Gross J (2012) The Functional Importance of Rhythmic Activity in the Brain. Current Biology 22: R658-R663.

Tiriac A, Uitermarkt BD, Fanning AS, Sokoloff G, Blumberg MS (2012) Rapid Whisker Movements in Sleeping Newborn Rats. Current Biology 22: 2075-2080.

Tritsch NX, Yi EY, Gale JE, Glowatzki E, Bergles DE (2007) The origin of

spontaneous activity in the developing auditory system. Nature 450: 50-+.

Tyzio R, Ivanov A, Bernard C, Holmes GL, Ben Ari Y, Khazipov R (2003) Membrane potential of CA3 hippocampal pyramidal cells during postnatal development. Journal of Neurophysiology 90: 2964-2972.

Ulrich D (2002) Dendritic resonance in rat neocortical pyramidal cells. Journal of Neurophysiology 87: 2753-2759.

van Brederode JFM, Berger AJ (2011) GAD67-GFP+ Neurons in the Nucleus of Roller. II. Subthreshold and Firing Resonance Properties. Journal of Neurophysiology 105: 249-278.

Vanderwolf CH (1988) Cerebral-Activity and Behavior - Control by Central Cholinergic and Serotonergic Systems. International Review of Neurobiology 30: 225-340.

Vinogradova OS (1995) Expression, Control, and Probable Functional-Significance of the Neuronal Theta-Rhythm. Progress in Neurobiology 45: 523-583.

Wagner J, Luhmann HJ (2006) Activation of metabotropic glutamate receptors induces propagating network oscillations in the intact cerebral cortex of the newborn mouse. Neuropharmacology 51: 848-857.

Wang HS, Pan ZM, Shi WM, Brown BS, Wymore RS, Cohen IS, Dixon JE, McKinnon D (1998) KCNQ2 and KCNQ3 potassium channel subunits: Molecular correlates of the M-channel. Science 282: 1890-1893.

Wang WT, Wan YH, Zhu JL, Lei GS, Wang YY, Zhang P, Hu SJ (2006) Theta-frequency membrane resonance and its ionic mechanisms in rat subicular pyramidal neurons. Neuroscience 140: 45-55.

Wilson MA, Mcnaughton BL (1994) Reactivation of Hippocampal Ensemble Memories During Sleep. Science 265: 676-679.

Winson J (1978) Loss of Hippocampal Theta Rhythm Results in Spatial Memory Deficit in Rat. Science 201: 160-163.

Wu NP, Hsiao CF, Chandler SH (2001) Membrane resonance and subthreshold membrane oscillations in mesencephalic V neurons: Participants in burst generation. J Neurosci 21: 3729-3739.

Yang JW, An S, Sun JJ, Reyes-Puerta V, Kindler J, Berger T, Kilb W, Luhmann HJ (2012) Thalamic Network Oscillations Synchronize Ontogenetic Columns in the Newborn Rat Barrel Cortex. Cereb Cortex.

Yang JW, Hanganu-Opatz IL, Sun JJ, Luhmann HJ (2009) Three Patterns of Oscillatory Activity Differentially Synchronize Developing Neocortical Networks In Vivo. J Neurosci 29: 9011-9025.

Zemankovics R, Kali S, Paulsen O, Freund TF, Hajos N (2010) Differences in subthreshold resonance of hippocampal pyramidal cells and interneurons: the role of h-current and passive membrane characteristics. Journal of Physiology-London 588: 2109-2132.

Zgraggen E, Boitard M, Roman I, Kanemitsu M, Potter G, Salmon P, Vutskits L, Dayer AG, Kiss JZ (2012) Early Postnatal Migration and Development of Layer II Pyramidal Neurons in the Rodent Cingulate/Retrosplenial Cortex. Cerebral Cortex 22: 144-157.

Zhang ZW (2004) Maturation of layer V pyramidal neurons in the rat prefrontal cortex: Intrinsic properties and synaptic function. Journal of Neurophysiology 91: 1171-1182.

Zhou FM, Hablitz JJ (1996) Postnatal development of membrane properties of layer I neurons in rat neocortex. J Neurosci 16: 1131-1139.

Zhu JJ (2000) Maturation of layer 5 neocortical pyramidal neurons: amplifying

salient layer 1 and layer 4 inputs by Ca2+ action potentials in adult rat tuft dendrites. Journal of Physiology-London 526: 571-587.

Ziskind-Conhaim L (2013) Neuronal correlates of the dominant role of GABAergic transmission in the developing mouse locomotor circuitry. Ann N Y Acad Sci 1279: 43-53.

Acknowledgments

I would like to express my great gratitude to my supervisor for giving me the opportunity to work in his lab.

I am very grateful to all supervisors and professors for reviewing my PhD defense.

Thanks to those who helped me on this manuscript.

Thanks to all colleagues of the lab for all the kinds of help.